J Physiol 589.17 (2011) pp 4301–4320

The Journal of Physiology

Presynaptic Ca^{2+} influx and vesicle exocytosis at the mouse endbulb of Held: a comparison of two auditory nerve terminals

Kun-Han Lin[1,2], Sharon Oleskevich[3] and Holger Taschenberger[1,2]

[1] *Max Planck Institute for Biophysical Chemistry, Am Fassberg 11, D-37077 Göttingen, Germany*
[2] *Sensory and Motor Neuroscience Program, Göttingen Graduate School for Neurosciences and Molecular Biosciences, Göttingen, Germany*
[3] *Garvan Institute of Medical Research, University of New South Wales, 384 Victoria Street, Darlinghurst-Sydney 2010, Australia*

Non-technical summary The release of neurotransmitter from presynaptic nerve endings is triggered by Ca^{2+} influx through voltage-gated Ca^{2+} channels (VGCCs) that open when an action potential (AP) invades the presynaptic terminal. The functional properties of VGCCs expressed in presynaptic terminals remain elusive because most terminals are too small to be accessible to electrophysiological recordings. We performed direct presynaptic recordings to characterize Ca^{2+} channels and transmitter release in a large mammalian presynaptic terminal, the endbulb of Held. Endbulb terminals are formed by the endings of auditory nerve fibres that contact bushy cells located in the anterior ventral cochlear nucleus. We find that endbulb terminals are endowed with >1000 readily releasable vesicles and express an average number of >6000 VGCCs. About half of the VGCCs open during a single AP. Thus, multiple Ca^{2+} channels control the release of a single transmitter vesicle at the endbulb of Held.

Abstract The functional properties of mammalian presynaptic nerve endings remain elusive since most terminals of the central nervous system are not accessible to direct electrophysiological recordings. In this study, direct recordings were performed for the first time at endbulb of Held terminals to characterize passive membrane properties, voltage-gated Ca^{2+} channels (VGCCs) and Ca^{2+}-dependent exocytosis. Endbulb of Held terminals arise from endings of auditory nerve fibres contacting spherical bushy cells (SBCs) in the anterior ventral cochlear nucleus (AVCN). These terminals had a high mean input resistance (1.1 GΩ) and a small mean capacitance (4.3 pF). Presynaptic VGCCs were predominantly of the P/Q type (86%) and expressed at a high density with an estimated average number of 6400 channels per terminal. Presynaptic Ca^{2+} currents ($I_{Ca(V)}$) activated and deactivated rapidly. Simulations of action potential (AP)-driven gating of VGCCs suggests that endbulb APs trigger brief Ca^{2+} influx with a mean half-width of 240 μs and a peak amplitude of 0.45 nA which results from the opening of approximately 2600 channels. Unlike Ca^{2+} currents at the calyx of Held, $I_{Ca(V)}$ of endbulb terminals showed no inactivation during trains of AP-like presynaptic depolarizations. Endbulb terminals are endowed with a large readily releasable vesicle pool (1064 vesicles) of which only a small fraction (<10%) is consumed during a single AP-like stimulus. Fast presynaptic APs together with rapidly gating VGCCs will generate brief intracellular Ca^{2+} transients that favour highly synchronous transmitter release. Collectively these characteristics ensure sustained and precise transmission of timing information from auditory stimuli at the endbulb→SBC synapse.

(Received 29 March 2011; accepted after revision 9 July 2011; first published online 11 July 2011)
Corresponding author H. Taschenberger: Max Planck Institute for Biophysical Chemistry, Am Fassberg 11, D-37077 Göttingen, Germany. Email: holger.taschenberger@mpi-bpc.mpg.de

Abbreviations AVCN, anterior ventral cochlear nucleus; MNTB, medial nucleus of the trapezoid body; RRP, readily rerleasable pool; SBC, spherical bushy cell; VGCC, voltage-gated Ca^{2+} channel.

DOI: 10.1113/jphysiol.2011.209189

Introduction

Synapses formed between the endings of auditory nerve fibres and bushy cells in the AVCN are the first relay centre in the mammalian auditory pathway. Specifically, the axons of spiral ganglion cells convey auditory sensory information from the inner hair cells to SBCs via large calyx-type axosomatic terminals – the endbulbs of Held. Spherical bushy cells carry timing information to the medial superior olivary nuclei, where the arrival time of sounds at the two ears is compared. Detailed reconstructions of endbulb→SBC connections have revealed that up to four endbulb terminals can contact single bushy cells (Brawer & Morest, 1975; Ryugo & Sento, 1991; Nicol & Walmsley, 2002). Similar to its larger cousin – the calyx of Held – each endbulb terminal can harbour hundreds of active zones with large clusters of synaptic vesicles (Neises *et al.* 1982; Ryugo *et al.* 1996, 1997; Nicol & Walmsley, 2002). The structural features of the endbulb synapse appear to facilitate the temporally precise transmission of spike activity of the auditory nerve which is believed to be a prerequisite for various tasks of auditory information processing (Rhode & Greenberg, 1992; Oertel, 1999; Young & Oertel, 2004).

Transmitter release from presynaptic endings is triggered by Ca^{2+} entering the cytoplasm through VGCCs that open when the AP invades the presynaptic terminal. Thus the shape of the action potential, together with the density and gating kinetics of presynaptically expressed VGCCs, critically determines synaptic strength as well as the timing of the release process. With only a few exceptions (Sivaramakrishnan & Laurent, 1995; Borst & Sakmann, 1998*a*; Forsythe *et al.* 1998; Bischofberger *et al.* 2002), the functional properties of presynaptic VGCCs have, however, largely remained *terra incognita*, owing to the small size of most presynaptic endings of the vertebrate brain.

Here we present the first direct recordings from mammalian endbulb of Held terminals of juvenile (P9–11) mice. To examine passive membrane properties, discharge properties and gating properties of presynaptic VGCCs, we made patch-clamp recordings from endbulb terminals in acute brain slices. We establish a Hodgkin–Huxley m^2 type kinetic scheme of presynaptic Ca^{2+} currents to simulate AP-driven Ca^{2+} influx at this synapse. Furthermore, we estimate the unitary current amplitude of VGCCs using variance–mean analysis to approximate the total number of presynaptic VGCCs expressed in a single endbulb terminal. In addition, we study the relation between Ca^{2+} influx and vesicle exocytosis using presynaptic capacitance measurements. Finally we compare these functional properties to those of calyx of Held terminals of the same developmental stage. Parts of this work were previously published in abstract form (Lin *et al.* 2010).

Methods

Slice preparation

Brainstem slices were prepared from C57BL/6N mice (P9–11) in accordance with animal care and use guidelines of the State of Lower Saxony as previously described (Erazo-Fischer *et al.* 2007). Briefly, mice were decapitated and the whole brain was quickly immersed into ice-cold low Ca^{2+} artificial CSF (aCSF) containing (in mM): 125 NaCl, 2.5 KCl, 3 $MgCl_2$, 0.1 $CaCl_2$, 10 glucose, 25 $NaHCO_3$, 1.25 NaH_2PO_4, 0.4 ascorbic acid, 3 *myo*-inositol, and 2 sodium pyruvate, pH 7.3. The brainstem was glued onto the stage of a VT1000S vibrating-blade microtome (Leica, Nussloch, Germany) and coronal slices (180–200 μm) containing the AVCN and/or medial nucleus of the trapezoid body (MNTB) were cut. Slices were incubated for ≥30 min at 35°C in an incubation chamber containing normal aCSF and kept at room temperature (22–24°C) for up to 4 h thereafter. The composition of normal aCSF was identical to low Ca^{2+} aCSF except that 1.0 mM $MgCl_2$ and 2.0 mM $CaCl_2$ were used. All solutions were oxygenated by continuous equilibration with carbogen gas (95% O_2, 5% CO_2).

Electrophysiology

Patch-clamp recordings were made from endbulb of Held terminals and SBCs of the AVCN, and calyx of Held terminals of the MNTB using an EPC-10 amplifier controlled by Pulse software (HEKA Elektronik, Lambrecht/Pfalz, Germany). Sampling intervals and filter settings were 20 μs and 4.5 kHz, respectively. Cells were visualized by differential interference contrast microscopy through a 60× water-immersion objective (NA 1.0, Olympus, Hamburg, Germany) using an Axioskop FS microscope (Zeiss, Oberkochen, Germany). All experiments were performed at room temperature.

Patch pipettes were pulled from borosilicate glass (Science Products GmbH, Hofheim, Germany) on a P-97 micropipette puller (Sutter Instrument Co., Novato, CA, USA). Pipettes were coated with dental wax to minimize fast capacitive transients during voltage-clamp experiments and to reduce stray capacitance. Open tip pipette resistance was 4–5 MΩ. Access resistance (R_s) values were ≤30 MΩ and ≤20 MΩ for recordings from endbulb and calyx terminals, respectively. R_s was compensated 50–60% during presynaptic voltage-clamp experiments.

For measuring presynaptic $I_{Ca(V)}$ and membrane capacitance (ΔC_m), pipettes were filled with a solution containing (in mM): 100 caesium gluconate, 30 TEA-Cl, 30 CsCl, 10 Hepes, 0.5 EGTA, 5 Na_2-phosphocreatine, 4 ATP-Mg, 0.3 GTP, pH 7.3 with CsOH. In some experiments 10 mM BAPTA was used and CsCl was

reduced to 10 mM. The bath solution was supplemented with 1 μM TTX, 1 mM 4-AP and 40 mM TEA-Cl to suppress voltage-gated sodium and potassium currents. For pharmacological dissection of $I_{Ca(V)}$, ω-agatoxin IVA (ω-AgaTX; 200 nM) (Alomone Labs, Jerusalem, Israel) was dissolved in aCSF containing 0.1 mg ml^{-1} cytochrome *c*. C_m was measured using the Sine+DC technique (Lindau & Neher, 1988) with a software lock-in amplifier (HEKA Pulse) by adding a 1 kHz sine wave voltage command (amplitude ±35 mV) to the holding potential (V_h) of −80 mV. To avoid a contamination of ΔC_m estimates after long-lasting presynaptic depolarizations with small C_m transients unrelated to vesicle exocytosis (Yamashita *et al.* 2005), ΔC_m was estimated from the averaged C_m values during 50 ms time windows immediately before and 450 ms after the end of the depolarizations. Presynaptic recordings with a leak current >150 pA were excluded from the analysis.

Presynaptic action potentials (APs) were elicited by either depolarizing current injections or afferent fibre stimulation. Stimulation pulses (100 μs duration) were applied using a stimulus isolator unit (A.M.P.I., Jerusalem, Israel), with the output voltage set to 1–2 V above threshold for AP generation (≤40 V). APs were measured in the current-clamp mode of the EPC-10 after carefully adjusting the fast-capacitance cancellation in cell-attached mode. For measuring APs, pipettes were filled with a solution containing (in mM): 100 potassium gluconate, 60 KCl, 10 Hepes, 5 EGTA, 5 Na_2-phosphocreatine, 4 ATP-Mg, 0.3 GTP, pH 7.3 with KOH. The presynaptic resting potential was close to −80 mV under these recording conditions. To facilitate comparison between different terminals, we adjusted V_m to −80 mV in all current-clamp recordings by injecting a small hyper- or depolarizing current. No liquid junction potential corrections (<10 mV) were applied.

Analysis of electrophysiological data

All off-line analysis was done with Igor Pro (WaveMetrics, Lake Oswego, OR, USA). Simulation of Ca^{2+} influx during an action potential was done using an m^2 Hodgkin–Huxley (HH) model (Hodgkin & Huxley, 1952; Borst & Sakmann, 1998a). This approach neglects any functional heterogeneities within the population of VGCCs (Wu *et al.* 1999; Li *et al.* 2007). For endbulb terminals, this should however not be a major complication because we found that ~86% of their $I_{Ca(V)}$ is mediated by P/Q-type Ca^{2+} channels (see below). Integrals of Ca^{2+} tail currents (500 μs) after 10 ms step depolarizations were used as a measure for steady-state activation (Augustine *et al.* 1985; Borst & Sakmann, 1998*a*). The voltage dependence of the average steady-state activation parameter m_∞^2 was obtained by fitting the normalized integrals with a squared Boltzmann function:

$$m_\infty^2 = 1/(1 + \exp((V_{0.5} - V_m)/\kappa))^2, \quad (1)$$

where V_m is membrane potential, $V_{0.5}$ is the half-activation voltage and κ is the steepness factor. The current–voltage (I–V) relation of $I_{Ca(V)}$ elicited by 10 ms steps was fitted with a product of the squared Boltzmann term and a modified form of the constant-field equation, giving the following function:

$$I(V_m) = m_\infty^2 P(V_m - V') \times \frac{\exp(-2V'/H)}{1 - \exp(2(V_m - V')/H)}, \quad (2)$$

where P, H and V' are constants determining current amplitude and rectification (Brown *et al.* 1983; see also Bischofberger *et al.* 2002).

For the construction of the HH m^2 model, deactivation of $I_{Ca(V)}$ during steps from 0 mV to voltages between −20 and −70 mV was fitted with single exponentials. The obtained time constants τ_f from exponential fits to the tail currents were then used to approximate the time constants of relaxation (τ_m) of the gate m after a voltage step using the following expression (Hagiwara & Ohmori, 1982; Sala, 1991):

$$\tau_f = \tau_m \times (m_\infty + m_0)/(2m_0). \quad (3)$$

Activation of $I_{Ca(V)}$ was measured during steps from $V_h = -80$ mV to potentials between −10 and +30 mV. The time course of current activation (0–3 ms after pulse onset) was fitted with a squared exponential function with delayed onset:

$$I(t) = I_\infty \times (1 - \exp(-(t - t_0)/\tau_m))^2, \quad (4)$$

where I_∞ is steady-state current and t_0 defines current onset.

Rate constants of the HH model, α_m and β_m, were then calculated from τ_m and m_∞ according to:

$$\alpha_m = m_\infty/\tau_m, \quad (5)$$

and

$$\beta_m = (1 - m_\infty)/\tau_m. \quad (6)$$

The dependences of α_m and β_m on V_m were fitted with exponential functions:

$$\alpha_m = \alpha_0 \times \exp(V_m/V_\alpha), \quad (7)$$

and

$$\beta_m = \beta_0 \times \exp(-V_m/V_\beta), \quad (8)$$

and the calculated rates α_m and β_m were used to estimate m during membrane depolarizations:

$$\frac{\partial m}{\partial t} = \alpha_m \times (1 - m) - \beta_m \times m. \quad (9)$$

The time course of the average activation parameter m was solved numerically using a fifth-order Runge–Kutta–Fehlberg algorithm implemented in Igor Pro and the simulated $I_{Ca(V)}$ was obtained from eqn (2) using the average parameters $P = 3.4\ \mu$S, $H = 12.9$ mV and $V' = 35.9$ mV and $P = 1.6\ \mu$S, $H = 19.3$ mV and $V' = 36.0$ mV for endbulb and calyx terminals, respectively.

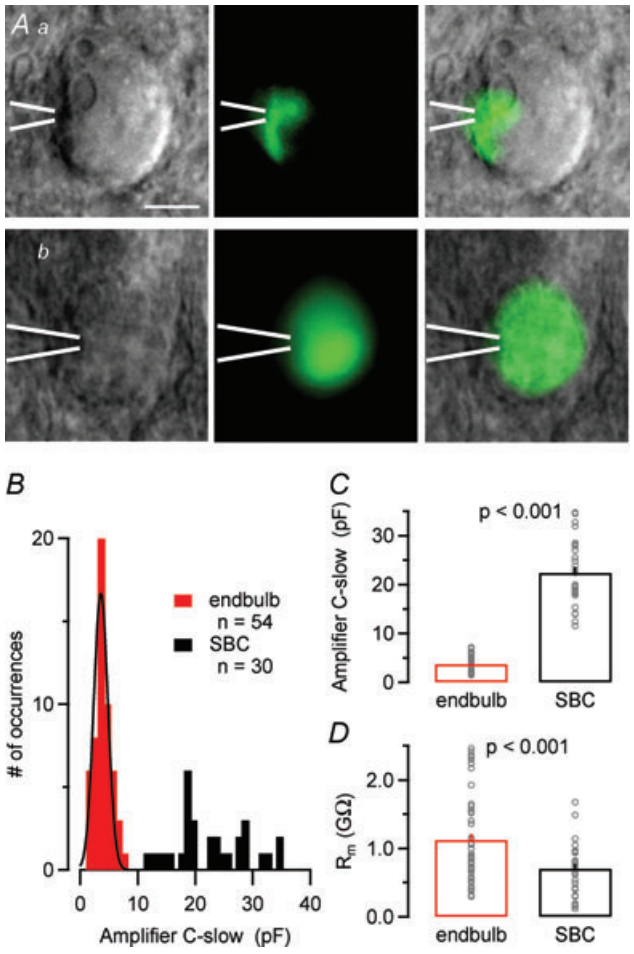

Figure 1. Unequivocal identification of endbulb of Held terminals
A, IR-DIC (left) and fluorescence (middle) images of spherical bushy cells in a brain slice taken after direct presynaptic (*Aa*) or postsynaptic (*Ab*) whole-cell recording. The intracellular recording solution contained a fluorescent dye. Overlays of both images are shown in the right column. Presynaptic recording sites were confirmed by exclusion of the fluorescent dye from the postsynaptic neurons. Position of the recording pipette as indicated by the white bars. Calibration bar corresponds to 10 μm. *B–D*, pre- and postsynaptic compartments can be easily distinguished by virtue of their divergent passive membrane properties. *B* and *C*, frequency distribution (*B*) and means (*C*) of the whole-cell capacitance (reading of the amplifier's *C*-slow cancellation setting) suggest a ~6 times smaller surface area for endbulb terminals compared to bushy cells. Note that the two frequency distributions in *B* do not overlap. The smooth black curve in *B* represents a Gaussian fit with a mean = 3.6 pF and SD = 1.7 pF. *D*, presynaptic terminals had higher input resistance than postsynaptic SBCs. R_m was determined from the passive current responses elicited by hyperpolarizing voltage steps from $V_h = -80$ to -90 mV.

For non-stationary ensemble fluctuation analysis of $I_{Ca(V)}$, records with identical pulse protocols (20 ms depolarizations to potentials between -19 and -8 mV) were taken every 3–5 s until a run of 20–151 current traces (on average 74 repetitions) was obtained. Next, we derived estimates for variance and mean, point by point, along a trace (Sigworth, 1980). The low-pass filtered ensemble variance $\sigma^2(t)$ of $I_{Ca(V)}$ was calculated from the $N-1$ difference traces between consecutive responses in order to optimally eliminate trends and drifts (Roberts *et al.* 1990; Heinemann & Conti, 1992):

$$\sigma^2(t) = \frac{1}{2(N-1)} \sum_{n=1}^{N-1} (\Delta I_n(t))^2 \qquad (10)$$

where $\Delta I_n(t)$ represent the nth difference trace $\Delta I_n(t) = I_n(t) - I_{n+1}(t)$ after off-line low-pass filtering using a 10-pole Bessel filter with a cut-off frequency $f_c = 2.5$ kHz. The ensemble mean $\bar{I}(t)$ of $I_{Ca(V)}$ was calculated according to:

$$\bar{I}(t) = \frac{1}{N} \sum_{n=1}^{N} I_n(t). \qquad (11)$$

Only in a few cases the variance–mean relationship showed unambiguous indications of deviation from linearity. Therefore, the single channel current of VGCCs was estimated from the slopes of regression lines fitted to the initial part of the variance–mean plots after subtracting the baseline variance σ_0^2 (see Fig. 7 for examples).

All values are given as means ± SEM. Significance of difference was evaluated by the two-tailed Student's unpaired t test. $P < 0.05$ was taken as the level of statistical significance.

Results

Identification of endbulb of Held terminals in acute mouse brainstem slices containing the AVCN

Using high-resolution differential interference contrast optics we were able to visualize and record from bouton-like structures surrounding the SBCs of the AVCN. These structures were identified as endbulb of Held terminals based on four distinct morphological and functional criteria: (i) small size, (ii) small whole-cell capacitance, (iii) high input resistance, and (iv) the presence of an increase in whole-cell capacitance (ΔC_m) reflecting vesicle exocytosis after eliciting presynaptic Ca^{2+} influx.

In a pilot set of experiments, patch-pipettes were filled with a fluorescent dye to validate our approach for identifying presynaptic recordings. Figure 1*A* shows

fluorescence images taken after recording from a presynaptic endbulb terminal and a postsynaptic SBC with pipettes containing a fluorescent dye. SBCs were identified by their large spherical somata with centrally located nuclei and a lack of prominent dendritic arborizations (Brawer *et al.* 1974; Cant & Morest, 1979; Wu & Oertel, 1984). During presynaptic recordings (Fig. 1*Aa*), the dye labelled terminals, but was clearly excluded from postsynaptic cells. Labelled terminals covered ≤25% of the bushy cell surface and their morphology resembled that of endbulb of Held terminals of young mice or kittens (Brawer & Morest, 1975; Ryugo & Fekete, 1982; Limb & Ryugo, 2000). Whole-cell membrane capacitance values were estimated from the automatic C_{slow} compensation setting of the EPC-10 amplifier from 54 endbulb terminals and 30 SBCs (Fig. 1*B* and *C*). The mean C_{slow} value was ∼6 times smaller for presynaptic terminals compared to postsynaptic cells (3.73 ± 0.18 *vs.* 22.40 ± 1.19 pF, $P < 0.001$, Fig. 1*C*) and the distributions of C_{slow} values did not overlap (Fig. 1*B*), thus illustrating the clear separation between pre- and postsynaptic recordings. In addition, endbulb terminals had an ∼60% higher mean input resistance when compared to SBCs (1.13 ± 0.09 GΩ, $n = 54$, *vs.* 0.71 ± 0.07 GΩ, $n = 30$, $P < 0.001$).

Passive membrane properties of endbulb and calyx of Held terminals

To compare the passive membrane properties of endbulb and calyx of Held terminals, we analysed capacitive current transients elicited by small hyperpolarizing voltage steps from $V_h = -80$ mV to −90 mV. To facilitate identification of presynaptic recordings, experiments were done under conditions that pharmacologically isolated voltage-gated Ca^{2+} currents and allowed time-resolved presynaptic capacitance measurements. Figure 2*A* illustrates $I_{Ca(V)}$ and the associated ΔC_m recorded from an endbulb and a calyx terminal. Passive current transients are shown in the bottom panels. The total capacitance of the entire presynaptic compartment (C_{total}) calculated from the current integrals was ∼3 times smaller for endbulb compared to calyx terminals (13.0 ± 0.9, $n = 54$, *vs.* 37.9 ± 1.8 pF, $n = 46$, $P < 0.001$). Passive current transients generally decayed bi-exponentially following voltage steps. The amplitude of the slowly decaying component was highly variable and most likely represented the slow charging of the membrane of the presynaptic axon of variable length (Borst & Sakmann, 1998a).

To estimate the surface area of the terminals, we fitted the passive capacitive current transients with bi-exponential functions and calculated the time integrals of the fast and slowly decaying current components presumably reflecting the membrane capacitance of the terminal ($C_{terminal}$) and that of the attached axon (C_{axon}), respectively (Fig. 2*B–D*). On average, the capacitance of endbulb terminals was ∼4 times smaller than that of calyces (Table 1) and little overlap between the two populations of C_m estimates was observed (Fig. 2*C*). In addition, $C_{terminal}$ estimates for endbulb terminals showed a significantly higher variability as indicated by their larger coefficient of variation (CV = 0.33 *vs.* 0.22, $P < 0.05$ by bootstrap analysis), suggesting a more variable size of endbulbs compared with calyx terminals. Interestingly, the estimated surface area of the presynaptic axons (C_{axon}) was also smaller for endbulbs compared to calyx terminals (8.6 ± 0.8 pF, $n = 54$, *vs.* 20.6 ± 1.7 pF, $n = 46$, $P < 0.001$, Fig. 2*D*). This is consistent with the idea that coronal slices may preserve a larger portion of the presynaptic axon for calyx synapses. The input resistance of both types of presynaptic terminals was very high (on average >1 GΩ, Fig. 2*E*, Table 1).

Properties of voltage-gated Ca^{2+} currents at endbulb and calyx terminals

The expression of VGCC subtypes at presynaptic terminals varies between different types of synapses (Luebke *et al.* 1993; Takahashi & Momiyama, 1993; Li *et al.* 2007). In addition, the expression of VGCC subtypes may be developmentally regulated: for example young calyces of Held express a mixture of P/Q-, N- and R-type VGCCs whereas mature terminals express nearly exclusively P/Q-type VGCCs (Iwasaki & Takahashi, 1998; Iwasaki *et al.* 2000). Application of the P/Q-type channel blocker ω-AgaTX reduced evoked EPSCs to <20% at P11–16 endbulb synapses suggesting that glutamate release is predominantly governed by P/Q-types already at this age (Oleskevich & Walmsley, 2002). To directly quantify the fractional expression of P/Q-type VGCCs in endbulbs, we measured the block by ω-AgaTX of pharmacologically isolated presynaptic $I_{Ca(V)}$ in endbulb synapses (Fig. 3*A*). Application of a saturating concentration of ω-AgaTX (200 nM) blocked ∼86% of $I_{Ca(V)}$. Only a minor fraction of $I_{Ca(V)}$ was insensitive to ω-AgaTX (13.8 ± 2.8%, $n = 3$).

To study voltage dependence of $I_{Ca(V)}$ in endbulb and calyx terminals, V_m was stepped from −80 mV to various potentials (10 ms duration, Fig. 3*B*). *I–V* relationships of $I_{Ca(V)}$ are illustrated in Fig. 3C for both terminals. The threshold for activation of $I_{Ca(V)}$ was around −40 mV, the *I–V* curves peaked between −10 and ±0 mV. The smooth curves in Fig. 3*C* represent fits to the *I–V* relationships using a modified form of the constant field equation (eqn (2), Brown *et al.* 1983; see also Bischofberger *et al.* 2002). Parameters from the fit were $P = 3.4$ μS, $H = 12.9$ mV and $V' = 35.9$ mV *versus* $P = 1.6$ μS, $H = 19.3$ mV and $V' = 36.0$ mV for endbulb and calyx terminals, respectively (Fig. 3*C*).

In endbulb terminals, $I_{Ca(V)}$ started to activate at slightly more negative V_m values. This is also reflected in a slight left shift of the corresponding steady-state activation curve obtained from the normalized integrals of Ca^{2+} tail currents (Fig. 3*D*). The voltage dependence of the steady-state activation parameter (m_∞^2) of calcium channels was fitted with a squared Boltzmann function (eqn (1)). Midpoint potentials of the steady-state activation curves (V_h) were −24.4 mV *vs.* −17.4 mV ($P < 0.001$), and the slope factors of the activation curve (κ) were 9.63 mV *versus* 8.23 mV ($P = 0.04$) for endbulb and calyx terminals, respectively (Fig. 3*D*).

To study current density of $I_{Ca(V)}$ in both types of presynaptic terminals, peak amplitudes of $I_{Ca(V)}$ were plotted *versus* terminal capacitance (Fig. 4*A*). Linear regression analysis indicated that the amplitude of $I_{Ca(V)}$ increased by ∼74 pA per picofarad membrane capacitance. On average, peak amplitudes of $I_{Ca(V)}$ were ∼3 times smaller in endbulbs compared to calyces (Fig. 4*B*), which is consistent with the much smaller size of the former terminals (see Fig. 2*B* and *C*, Table 1). Interestingly, mean Ca^{2+} current densities were slightly larger in endbulbs (Fig. 4*C*). In both cases, Ca^{2+} current densities were comparable to previously reported values for calyces in P8–10 rats (Borst &

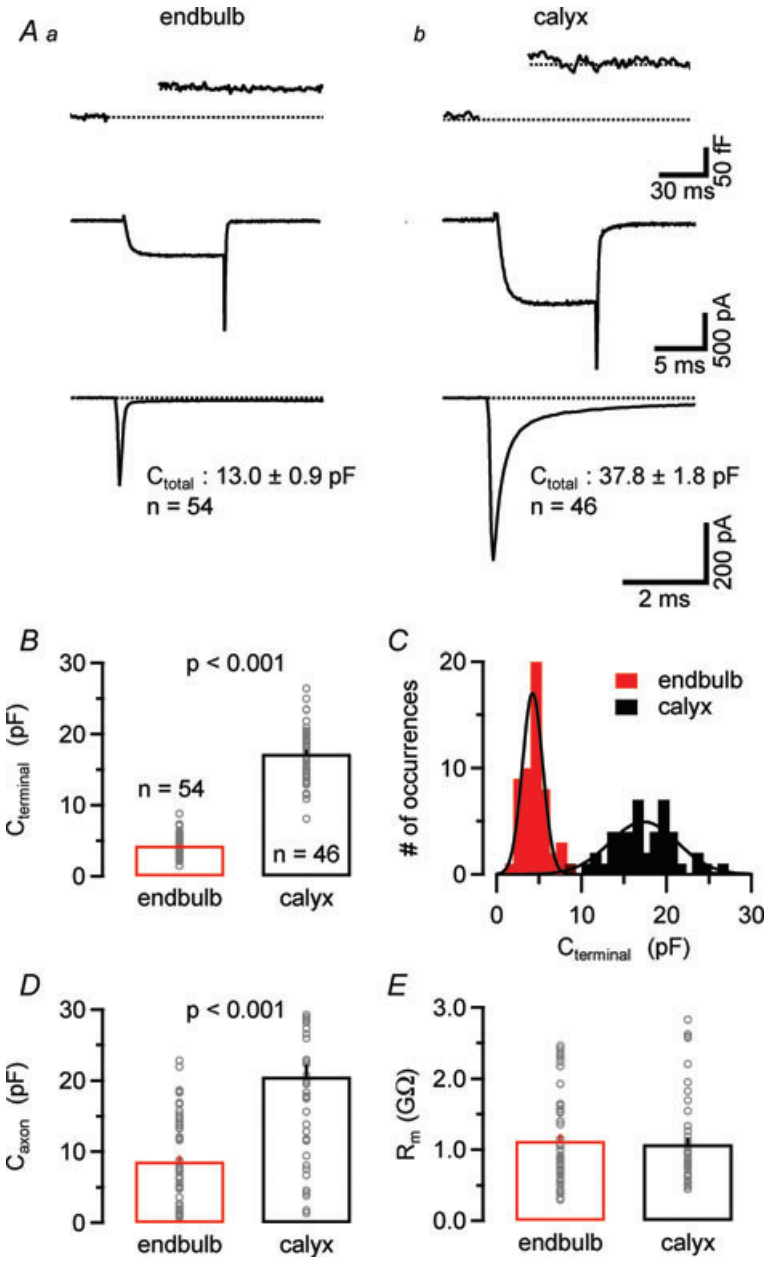

Figure 2. Comparison of passive membrane properties between endbulb and calyx terminals
A, changes in membrane capacitance (ΔC_m, top panel) elicited by step-depolarizations (10 ms, from $V_h = -80$ to 0 mV). The corresponding $I_{Ca(V)}$ are shown in the middle panel. The total resting membrane capacitance of the terminals (C_{total}) was estimated from integrals of passive current transients elicited by hyperpolarizing steps to –90 mV (bottom) recorded in whole-cell voltage clamp after compensating the pipette's capacitance in cell-attached mode. C_{total} was on average ∼3 times smaller for endbulb terminals. Capacitive current transients of most terminals decayed double exponentially suggesting a variable contribution of the attached axon to the total membrane capacitance. *B–D*, to distinguish the whole-cell capacitance of the terminals ($C_{terminal}$, *B* and *C*) from that of the attached axons (C_{axon}, *D*), we separated the capacitive current transients into fast and slowly decaying components. On average, endbulb terminals had a ∼4 times smaller $C_{terminal}$ (*B*) with a larger coefficient of variation (*C*) suggesting more variable size of these terminals. The smooth black curves in *C* represent Gaussian fits with means of 4.25 pF *vs.* 17.3 pF and SDs of 1.68 pF *vs.* 5.63 pF for endbulb and calyces, respectively. *E*, input resistance was on average ≥1 MΩ for both endbulb and calyx terminals.

Table 1. Comparison of functional properties of endbulb of Held (P9–P11) and calyx of Held (P8–P11) terminals of mice

	Endbulb P9–P11	Calyx P8–P11	Significance level (*P*)
Passive membrane properties			
$C_{terminal}$ (pF)	4.3 ± 0.2(54)	17.2 ± 0.6(46)	<0.001
C_{axon} (pF)	8.6 ± 0.8(54)	20.6 ± 1.7(46)	<0.001
R_m (GΩ)	1.13 ± 0.09(54)	1.08 ± 0.09(46)	n.s.
Presynaptic $I_{Ca(V)}$			
Amplitude (nA)[a]	−0.42 ± 0.03(28)	−1.29 ± 0.05(36)	<0.001
Current density (nA pF^{-1})	−0.105 ± 0.008(28)	−0.076 ± 0.003(36)	0.001
Inactivation during 100 ms (%)[b] (0.5 mM EGTA)	31.7 ± 2.0(14)	44.5 ± 1.8(18)	<0.001
Inactivation during 100 ms (%) (10 mM BAPTA)	18.7 ± 1.8(9)	37.2 ± 1.1(13)	<0.001
Unitary current at 0 mV (pA)	0.08 ± 0.01(8)	0.08 ± 0.00(10)	n.s.
Unitary slope conductance (pS)	1.85 ± 0.16(8)	1.80 ± 0.1(10)	n.s.
Ca^{2+} channels/terminal[d]	6367 ± 498(28)	20, 438 ± 801(36)	<0.001
Presynaptic APs			
AP amplitude (mV)	122.0 ± 5.1(5)	130.5 ± 0.8(5)	n.s.
AP half-width (μs)	262.8 ± 14.7(5)	356.3 ± 19.2(5)	<0.05
Vesicle exocytosis			
RRP from ΔC_m[c]	1064 ± 143(7 − 11)	2963 ± 184(9)	
$I_{Ca(V)}$ (nA)	−0.48 ± 0.05(7)	−1.29 ± 0.06(9)	<0.001
Ca^{2+} channels/vesicle in RRP	7.6 ± 1.2(7)	6.8 ± 0.6(9)	n.s.

[a]Peak amplitude of $I_{Ca(V)}$ evoked by a 10 ms step depolarization from −80 mV to 0 mV. [b]Inactivation of Ca^{2+} current during the 100 ms step depolarization to 0 mV was expressed as $(I_{peak}-I_{100ms})/I_{peak}$. [c]Size of the RRP was estimated by capacitance measurements. ΔC_m values were converted into vesicle numbers by assuming a single vesicle capacitance of 80aF. SEM was estimated by bootstrap analysis using 10,000 replications. [d]Estimates for the total number of VGCCs are derived by dividing $I_{Ca(V)}$ by the product of unitary current amplitude and the open probability at $V_m = 0$ mV.

Sakmann, 1998*a*) or rat hippocampal mossy fibre terminal (Bischofberger *et al.* 2002).

Establishing an HH-type m^2 model of $I_{Ca(V)}$ in endbulb terminals

We next studied activation and deactivation kinetics of $I_{Ca(V)}$ with the aim of establishing a simple HH-type m^2 model to simulate Ca^{2+} influx during presynaptic AP activity. Rapid voltage clamp is critical for determining the gating kinetics of VGCCs. Voltage-clamp speed is limited by the kinetics of the charging of the terminal, which occurs with a time constant $\tau = R_s \times C_{terminal}$, where R_s is the uncompensated series resistance and $C_{terminal}$ is the terminal capacitance. Mean time constants were 34 μs and 88 μs for endbulb and calyx recordings, respectively. Figure 5*Aa* illustrates a family of $I_{Ca(V)}$ elicited by 10 ms voltage steps to V_m between −10 and +30 mV. $I_{Ca(V)}$ activated very rapidly with time constants <1 ms when fitted with single exponentials. Average activation time constants (τ_A) were 0.84, 060, 0.45, 0.33 and 0.32 ms for steps to −10, ±0, 10, 20 and 30 mV, respectively ($n = 10$). The activation time constants of the m gate (τ_m) were obtained from fitting the current onset with eqn (4). Deactivation of $I_{Ca(V)}$ was studied by analysing Ca^{2+} tail currents elicited by 10 ms depolarizations to 0 mV followed by steps to V_m between −20 and −70 mV (Fig. 5*A2*). Some experiments in which $I_{Ca(V)}$ was followed by slow tail currents, possibly reflecting axonal Ca^{2+} conductances (Borst & Sakmann, 1998a), were excluded from the analysis. Decay time constants derived from single exponential fits to Ca^{2+} tail currents (τ_D) were 0.10, 0.13, 0.18, 0.26, 0.39 and 0.51 ms in endbulb ($n = 10$) *vs.* 0.12, 0.14, 0.17, 0.24, 0.40, and 0.63 ms in calyx terminals ($n = 12$) for steps to −70, −60, −50, −40, −30 and −20 mV, respectively. The deactivation time constants τ_m were estimated from τ_D according to eqn (3) and plotted together with those derived from activation of $I_{Ca(V)}$ (Fig. 5*B*). The bell-shaped dependence of τ_m on membrane potential is expected for a voltage-gated channel. The corresponding opening (α_m) and closing (β_m) rates were then calculated from the steady-state activation parameter m^2_∞ and τ_m, and their voltage dependence was fitted with single exponential functions (Fig. 5*C*). Table 2 summarizes model parameters for presynaptic $I_{Ca(V)}$ in mouse endbulb and calyx terminals.

To validate our HH-type m^2 model for endbulb VGCCs, we compared the experimentally recorded $I_{Ca(V)}$ elicited by a 1 ms depolarization to 0 mV with the predicted one (Fig. 5*D*). The simulated voltage step was low-pass filtered with a single-pole filter having a relaxation time constant as predicted by the measured values for membrane capacitance and series resistance (Fig. 5*D* top panel). The time course of the activation parameter m^2 is shown in

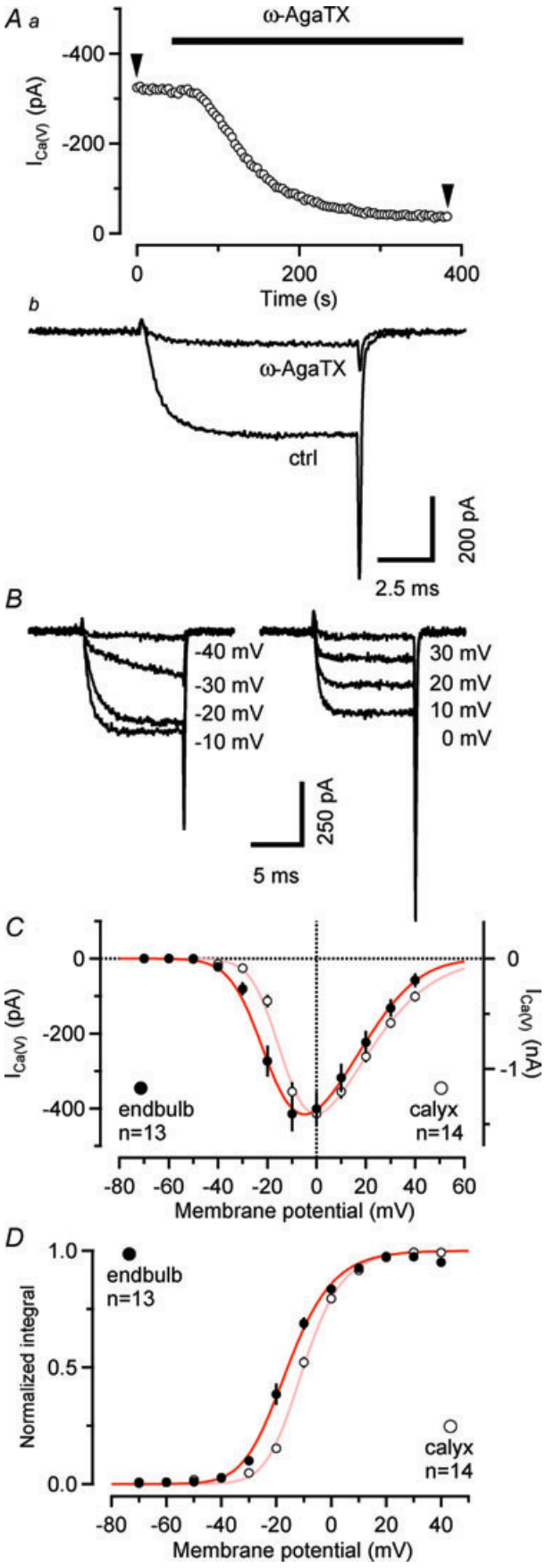

the middle panel. Its peak value was ~0.71. Except for the absence of the small outward transient at current onset, possibly reflecting a gating current, and a small deviation at the end of the deactivation time course, the simulated $I_{Ca(V)}$ (red trace) closely matched the measured one (bottom panel).

Simulating Ca^{2+} influx following presynaptic APs

The presynaptic AP waveform is a key parameter for determining presynaptic Ca^{2+} influx and thereby vesicle release (Llinas *et al.* 1982; Augustine, 1990; Sabatini & Regehr, 1997; Borst & Sakmann, 1999). Presynaptic APs in calyx terminals are very fast (Barnes-Davies & Forsythe, 1995; Borst *et al.* 1995) and their time course is further accelerated during synapse maturation (Taschenberger & von Gersdorff, 2000; Erazo-Fischer *et al.* 2007). In order to determine the presynaptic AP waveform in endbulb terminals we used two approaches. Firstly, we depolarized the terminals under current-clamp by injecting sustained or pulse-like depolarizing currents. Secondly, we stimulated the afferent fibres and recorded the shape of the invading presynaptic AP.

Figure 6 compares changes in membrane voltage in response to injection of sustained hyper- or depolarizing currents (Fig. 6*Aa*), pulse-like depolarizing currents (Fig. 6*Ab*) or a train of afferent-fibre stimuli (Fig. 6*Ac*). For comparison, the waveforms of the first AP in the trains are shown at a faster time scale in Fig. 6*B*. In response to sustained depolarizing currents, endbulb terminals generally generated only a single AP (two APs in 1 out of 14 terminals tested), similar to reports for P13–15 rat calyces (Nakamura & Takahashi, 2007). As expected from a synapse that is able to transmit at high frequency (Joris *et al.* 1994), endbulb terminals fired reliably at

Figure 3. Properties of voltage-gated Ca^{2+} currents in endbulb terminals
A, P/Q-type VGCC account for ~86% of $I_{Ca(V)}$ in endbulb terminals. $I_{Ca(V)}$ was elicited every 3.9 s by depolarizing voltage steps (10 ms, from V_h = –80 to 0 mV) while ω-AgaTX (200 nM) was applied to the external solution as indicated by the bar. Time course of block (*Aa*) and individual sweeps (*Ab*) representing the amplitude values at arrowheads. *B* and *C*, current–voltage relationship of $I_{Ca(V)}$ in endbulb and calyx terminals. *B*, $I_{Ca(V)}$ was elicited in an endbulb terminal by step depolarizations (10 ms duration) from V_h = –80 mV to the potentials indicated next to each trace. *C*, *I–V* curves obtained from peak amplitudes of $I_{Ca(V)}$ from 13 endbulb (black) and 14 calyx (grey) terminals. The smooth red curves represent fits to the data points using a modified form of the constant-field equation (see Methods eqn (2)). *D*, normalized tail current integrals of 10 ms step depolarizations plotted as a function of V_m to estimate the steady-state activation parameter m^2_∞. The smooth red curves represents fits to the data points using a squared Boltzmann function with half-activation voltages $V_{0.5}$ = –24.4 mV (endbulb) and –17.4 mV (calyx) and steepness factors κ = 9.63 mV (endbulb) and 8.23 mV (calyx).

high frequency when stimulated with either trains of pulse-like depolarizations or by trains of afferent fibre stimuli. AP peak amplitudes were similar when evoked by either current injection or afferent fibre stimulation (121.4 ± 2.7 mV, $n = 10$, *versus* 122.0 ± 5.1 mV, $n = 5$, $P = 0.92$) (Fig. 6*C*). Surprisingly, the duration of endbulb APs was ∼65% longer when elicited by current injection (432.5 ± 29.2 μs, $n = 10$, *vs.* 262.8 ± 14.7 μs, $n = 5$, $P < 0.001$) (Fig. 6*B* and *C*). We therefore decided to use AP waveforms recorded after fibre stimulation exclusively in the simulation described below.

In order to estimate $I_{Ca(V)}$ during single presynaptic APs at endbulb terminals, we used the recorded AP waveforms to drive the HH-type m^2 model of $I_{Ca(V)}$ described above. The estimate of endbulb AP-driven Ca^{2+} influx was then compared to that in calyx terminals. Typical presynaptic APs from an endbulb and a calyx are shown superimposed in Fig. 6*E*. Presynaptic APs of both auditory terminals are much briefer than those recorded in hippocampal mossy-fibre boutons (half-width 852 μs at room temperature, Bischofberger *et al.* 2002). On average, the duration of endbulb APs was ∼26% shorter compared to calyx APs, and their peak amplitude was ∼7% lower (Table 1). This suggests that endbulb APs may open presynaptic VGCCs less effectively than calyx APs recorded at the same age. Figure 6*F* shows that this is indeed the case: the average peak value of m^2 was substantially lower in endbulb compared to calyx terminals (Table 2). Taken together, our simulations estimate that AP-driven Ca^{2+} influx is greatly reduced (∼6 times less) in endbulb compared to calyx terminals. In addition, the half-width of $I_{Ca(V)}$ during presynaptic APs was ∼13% shorter in endbulb compared to calyx terminals (Fig. 6*G*, Table 1). Peak amplitudes and charge of the simulated $I_{Ca(V)}$ during presynaptic APs reported here for the P9–P11 mouse calyx of Held are slightly smaller than the values previously reported for P8–P10 rat calyces of Held (Borst & Sakmann, 1998*a*).

Estimating the total number of VGCCs expressed at endbulb and calyx terminals

Estimating the total number of VGCCs expressed at endbulb and calyx synapses requires knowledge about their unitary current amplitude (i) and open probability (p_o). We therefore set out to obtain estimates of i from non-stationary fluctuation analysis of presynaptic $I_{Ca(V)}$ (Sigworth, 1980; Brandt *et al.* 2005; Li *et al.* 2007). To facilitate the analysis of current fluctuations around mean currents of variable amplitudes, we elicited $I_{Ca(V)}$ by 20 ms steps to relatively low V_m values (−19 to −8 mV), which resulted in relatively slowly activating currents. Such stimuli also avoided the contamination of the rising phase of $I_{Ca(V)}$ with outward 'asymmetry' currents that were reported earlier by Borst & Sakmann (1998*a*) and generally seen at current onset. Sets of 20–151 (on average 74) identical, 20 ms depolarizations were applied. Families of successively recorded $I_{Ca(V)}$ are shown in Fig. 7 for an endbulb (Fig. 7*A*) and a calyx (Fig. 7*B*) terminal. The rising phase of the Ca^{2+} currents was associated with a marked variance increase. Variance–mean plots are shown in the bottom panels of Fig. 7*A*–*C*. Using line fits to the initial portion of these plots, we thus estimated the unitary current amplitude i to be −0.117 pA and −0.130 pA for the two terminals illustrated in Fig. 7. To verify that the observed increase in variance originated from stochastic gating of VGCCs, we repeated the experiments in the presence of elevated external Ca^{2+} (6 mM). Consistent with the expected increase in Ca^{2+} flux, i increased more than

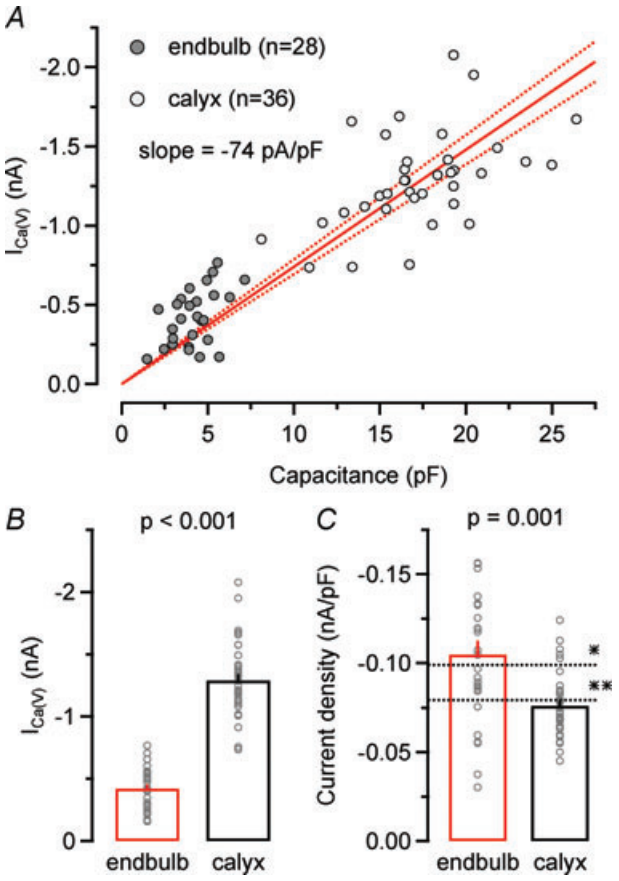

Figure 4. Ca^{2+} current densities are slightly larger in endbulb *versus* calyx terminals
A, scatter plot of $I_{Ca(V)}$ *versus* terminal capacitance obtained from 28 endbulb and 36 calyx terminals. $I_{Ca(V)}$ was elicited by step depolarizations to $V_h = 0$ mV. Continuous and dotted red lines represent linear regression and 95% confidence intervals for the entire data set, respectively. The slope of the regression line was −74 pA pF^{-1}. *B* and *C*, average amplitudes (*B*) and current densities (*C*) of $I_{Ca(V)}$ in endbulb and calyx terminals. For comparison, current densities for rat calyces (Borst & Sakmann, 1998a) (*) and rat hippocampal mossy fibre terminal (Bischofberger *et al.* 2002) (**) are indicated by the dotted lines.

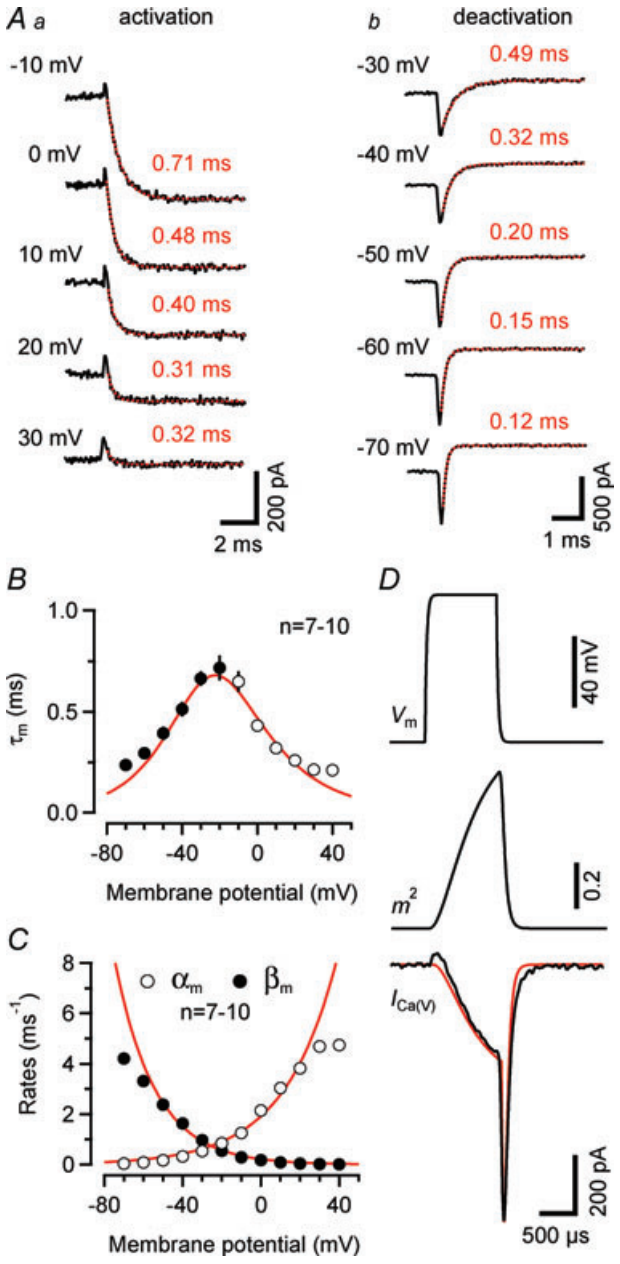

Figure 5. Hodgkin–Huxley model of Ca^{2+} influx in endbulb terminals
A, rapid activation (*Aa*) and deactivation (*Ab*) kinetics of $I_{Ca(V)}$. Smooth red curves represent single exponential fits. *Aa*, activation of $I_{Ca(V)}$ elicited by depolarizing voltage steps from $V_h = -80$ mV to various V_m values ($\tau_A = 0.71$, 0.46, 0.40, 0.31 and 0.32 ms for steps to –10, 0, 10, 20 and 30 mV, respectively). *Ab*, deactivation of $I_{Ca(V)}$ after a 10 ms depolarization to 0 mV after stepping back to various V_m values ($\tau_D = 0.49$, 0.32, 0.20, 0.15 and 0.12 ms for steps to –30, –40, –50, –60 and –70 mV, respectively). *B*, time constants τ_m measured from deactivation (–70 to –20 mV, eqn. 3, filled circles) or activation (–10 to 40 mV, eqn. 4, open circles) of $I_{Ca(V)}$. The smooth line represents the time constants predicted from the rate constants of the HH-model ($\tau_m = 1/(\alpha_m + \beta_m)$). *C*, activation ($\alpha_m$) and deactivation ($\beta_m$) rates of the gate m plotted as a function of V_m. Continuous lines are single exponential fits (eqns (7) and (8)), with $\alpha_0 = 2.03\ ms^{-1}$, $V_\alpha = 26.5$ mV and $\beta_0 = 0.22\ ms^{-1}$, $V_\beta = 19.8$ mV. Potentials >20 and <−60 mV were excluded from the fit. *D*, comparison of measured and simulated $I_{Ca(V)}$ elicited by a 1 ms depolarization to 0 mV. The assumed time course of V_m (top panel) was obtained by digitally filtering a 1 ms step with a single-pole filter (time constant $\tau = R_s \times C_m$, where R_s and C_m represent uncompensated series resistance and whole-cell capacitance, respectively). The activation parameter m^2 peaked at ~0.71 (middle panel). Except for a small deviation at the end of the deactivation time course, the simulated $I_{Ca(V)}$ (red trace) closely matched the measured current (black trace, bottom panel).

twofold (−0.309 pA for the terminal illustrated in Fig. 7*C*) under these conditions.

An expression relating i to the expected unitary current amplitude at $V_m = 0$ mV ($i(0)$) can be obtained from eqn (2):

$$\frac{i}{i(0)} = \frac{(V_m - V') \times (\exp(2V'/H) - 1)}{V' \times (\exp(2V_m/H) - \exp(2V'/H))}. \quad (12)$$

Average values for $i(0)$ were similar for endbulb and calyx terminals (Fig. 7*D*, Table 1), but smaller than those previously estimated for hippocampal mossy fibre boutons (Li *et al.* 2007). Using these unitary current amplitudes, we estimate that an average number of 5500 *versus* 16,400 VGCCs open at the peak of 0 mV depolarizations in endbulb and calyx terminals, respectively. We estimate an average total number of 6400 channels (endbulb) *versus* 20,400 channels (calyx) are expressed in these presynaptic terminals, assuming that the macroscopic steady state activation parameter m^2 (Fig. 3*Bc*) reflects the microscopic channel open probability (endbulb $m^2(0) = 0.86$, calyx $m^2(0) = 0.80$).

$I_{Ca(V)}$ inactivation and facilitation in endbulb and calyx terminals

During sustained membrane depolarizations or high-frequency trains of short, AP-like depolarizations, the presynaptic $I_{Ca(V)}$ in calyx terminals shows prominent current inactivation (Forsythe *et al.* 1998). Since transmitter release is highly non-linearly related to calcium influx (Neher, 1998), even minute changes in presynaptic Ca^{2+} flux can strongly modulate vesicle release. Indeed, inactivation of $I_{Ca(V)}$ during repetitive presynaptic AP firing has been suggested to account for a sizable fraction of synaptic depression at the calyx of Held (Xu & Wu, 2005; but see Nakamura *et al.* 2008). In Fig. 8*A*, $I_{Ca(V)}$ inactivation during 100 ms depolarizations to 0 mV is compared between endbulb and calyx terminals. Significantly less inactivation of $I_{Ca(V)}$ was observed in the endbulb terminals (Fig. 8*Ab*, Table 1). Since $I_{Ca(V)}$ inactivation is at least partially Ca^{2+} dependent, we quantified $I_{Ca(V)}$ inactivation in the presence of a high intracellular concentration of the Ca^{2+} chelator BAPTA.

Table 2. Parameters of the HH-type m^2 model of presynaptic $I_{Ca(V)}$ used to simulate AP-driven presynaptic Ca^{2+} influx in endbulb and calyx terminals

	Endbulb P9–P11	Calyx P8–P11
HH-model parameters		
Half-activation voltage (mV)	24.35	17.37
Steepness factor κ (mV)	9.63	8.23
α_0 (ms^{-1})	1.9135	1.5012
V_α (mV)	26.81	20.51
β_0 (ms^{-1})	0.2146	0.2384
V_β (mV)	20.55	20.85
P (μS)	3.3967	1.5916
H (mV)	12.912	19.264
V' (mV)	35.913	32.955
Simulated $I_{Ca(V)}$ during single presynaptic APs[a]		
Peak m^2	0.49 ± 0.06 (5)	0.88 ± 0.01 (5)
Amplitude (nA)	−0.45 ± 0.06 (5)	−2.78 ± 0.02 (5)
Current density (nA pF^{-1})	−0.105 ± 0.013 (5)	−0.161 ± 0.001 (5)
$Q_{Ca(V)}$ (pC)	−0.11 ± 0.01 (5)	−0.82 ± 0.03 (5)
Half-width (μs)	240 ± 15 (5)	276 ± 13 (5)
Open Ca^{2+} channels at peak	2616 ± 318 (5)	16,405 ± 136 (5)

[a]AP waveforms recorded in 5 endbulb and 5 calyx terminals were used to simulate AP-evoked Ca^{2+} influx.

Interestingly, $I_{Ca(V)}$ inactivation was further reduced under these conditions in endbulb terminals but nearly unaffected in calyx terminals (Fig. 8*B*). The steady-state inactivation of $I_{Ca(V)}$ was nearly negligible in both endbulb and calyx terminals (≤18% for conditioning potentials between –120 mV and –40 mV, $n = 7$) (Fig. 8*C*). We can thus exclude the possibility that stronger resting-state inactivation accounts for the reduced inactivation of $I_{Ca(V)}$ during 100 ms steps in endbulb compared to calyx terminals.

To investigate if $I_{Ca(V)}$ inactivation during presynaptic AP activity varies with auditory nerve firing frequency, we delivered trains consisting of 25 AP-like depolarizations (1 ms from $V_h = -80$ to 0 mV, Fig. 9) at various frequencies. Figure 9*A* illustrates the resulting $I_{Ca(V)}$ trains recorded in an endbulb (Fig. 9*A*1) and a calyx (Fig. 9*A*2) elicited at a frequency of 200 Hz (Fig. 9*A* left panels). During the first two to three stimuli, $I_{Ca(V)}$ facilitated (Borst & Sakmann, 1998b; Cuttle *et al.* 1998). Its peak amplitude remained stable thereafter in the endbulb but decreased in the calyx terminal. First and last $I_{Ca(V)}$ of the 200 Hz trains are shown superimposed for comparison (Fig. 9*A* middle panels). In contrast, during 10 Hz stimulation, $I_{Ca(V)}$ remained stable throughout the train in the endbulb but inactivated in the calyx (Fig. 9*A* right panels). Summary results for various train frequencies ranging from 1 to 200 Hz are compared in Fig. 9*B*. $I_{Ca(V)}$ inactivation was completely absent from endbulb terminals for all frequencies tested (Fig. 9*Ba*). $I_{Ca(V)}$ facilitation was observed for frequencies ≥20 Hz and peaked at a level of ∼20%. Calyces of Held, on the other hand, showed robust $I_{Ca(V)}$ inactivation during low-frequency stimulation (≤10 Hz). For frequencies ≥20 Hz, calyceal $I_{Ca(V)}$ showed net facilitation during the onset of the stimulus train whereas $I_{Ca(V)}$ inactivation dominated the remainder of the train (Fig. 9*Bb*).

Ca^{2+}-dependent vesicle exocytosis assayed by ΔC_m measurements in endbulb and calyx terminals

We used capacitance measurements to quantify and compare Ca^{2+}-dependent vesicle release in endbulb and calyx terminals (Sun & Wu, 2001; Taschenberger *et al.* 2002). Figure 10*A* shows families of $I_{Ca(V)}$ and corresponding changes in C_m that were elicited by variable-length depolarizations to 0 mV lasting between 2 and 50 ms for an endbulb (Fig. 10*Aa*) and a calyx terminal (Fig. 10*Ab*). Capacitance jumps evoked by depolarizations shorter than 2 ms were difficult to resolve in endbulb terminals. The 2 ms depolarization elicited ΔC_m of 17.9 fF and 51.0 fF in the endbulb and calyx, respectively. Assuming a mean vesicle diameter of ∼50 nm (Ryugo *et al.* 1996; Taschenberger *et al.* 2002) and a specific membrane capacitance of 10 fF μm^{-2}, we estimate an average capacitance of ∼80 aF for a single vesicle. Capacitance jumps measured in response to 2 ms depolarizations thus correspond to the release of ∼220 (endbulb) *vs.* ∼640 (calyx) vesicles. Longer depolarizations induced larger capacitance jumps. But the increase in ΔC_m became

smaller or saturated for pulse durations ≥40 ms suggesting depletion of a readily releasable pool of vesicles. In the terminals illustrated in Fig. 10*A*, 50 ms steps increased C_m by 77.7 fF (971 vesicles) and 271.9 fF (3399 vesicles) in the endbulb and calyx terminals, respectively.

Pooled data obtained from 7–11 endbulb and nine calyx terminals are plotted as a function of pulse duration or Ca^{2+} current charge in Figs 10*B* and *C*, respectively. Single exponentials fitted to the relationship between ΔC_m and pulse duration yielded time constants of 10.2 ms *vs.* 13.2 ms for endbulbs and calyces, respectively. These values are similar to a 'weighted' time constant of vesicle depletion obtained from deconvolution analysis of post-synaptic currents at the calyx synapse when using the same pipette concentration of EGTA (11.1 ms, Sakaba & Neher, 2001). About half of the readily releasable vesicles were consumed after 7.1 ms *versus* 9.2 ms pulse durations in the endbulb and calyx terminals, respectively. Faster time constants of release have been observed in the presence of lower concentrations of internal Ca^{2+} buffers (Sakaba & Neher, 2001; Sun & Wu, 2001). Moreover, release probability is heterogeneous at the calyx (Sakaba & Neher, 2001) and other central synapses (Walmsley *et al.* 1988; Hessler *et al.* 1993; Rosenmund *et al.* 1993; Murthy *et al.* 1997). When fitted with double exponential functions, the fast components of vesicle depletion had time constants

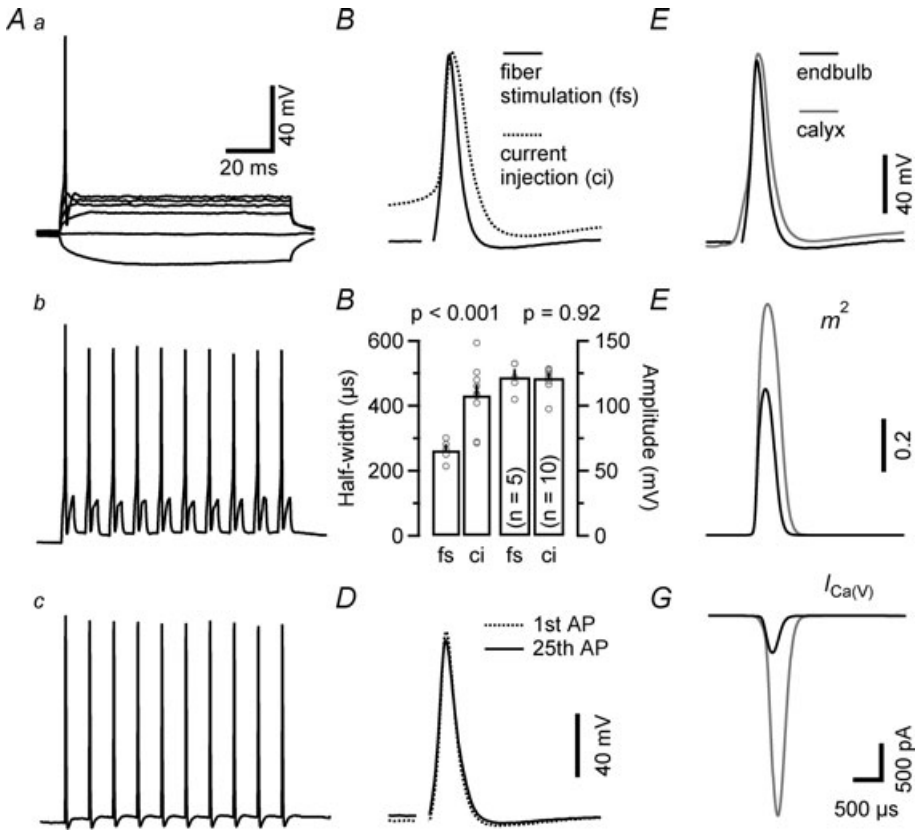

Figure 6. Ca^{2+} influx during a single presynaptic action potential is significantly less at endbulb *versus* calyx terminals

A, presynaptic membrane potential responses to either sustained (*Aa*, 100 ms duration, –30 to 120 pA) or pulse-like (*Ab*, 1 ms duration, 180 pA) current injections recorded in current-clamp configuration. *B*, comparison of presynaptic APs elicited by current injection of afferent fibre stimulation. Initial APs from the trains illustrated in *Ab* and *Ac* shown superimposed. *C*, presynaptic APs elicited by afferent fibre stimulation had shorter half-widths (left) but similar peak amplitudes (right) when compared with those elicited by depolarizing current injections. *D*, first and last APs elicited by a 100 Hz train consisting of 25 stimuli are shown superimposed to illustrate stability of AP waveform during high-frequency stimulation. *E–G*, comparison of simulated $I_{Ca(V)}$ during presynaptic endbulb and calyx APs. *E*, endbulb APs (black) were slightly smaller in amplitude and shorter in duration compared to those recorded from calyxes (grey). *F*, simulated time course of the activation parameter m^2. Because of its larger amplitude and longer duration, the calyceal AP waveform opened presynaptic VGCC more efficiently than the endbulb AP. *G*, simulated $I_{Ca(V)}$ during presynaptic APs in endbulb (black) and calyx (grey) AP. On average, the simulated presynaptic $I_{Ca(V)}$ was ∼6 times smaller for endbulb terminals compared to the simulated current for calyx terminals. The time scale bars in panels *Aa* and *G* also apply to panels *Ab*, *Ac* and *B*, *D*, *E* and *F*, respectively. V_m was −80 mV.

of 4.49 ms (endbulb) and 4.46 ms (calyx), which is slightly slower than those obtained from deconvolution analysis of calyceal EPSCs (Sakaba & Neher, 2001).

The average size of the readily releasable pool, obtained from the exponential fits, amounted to 85.1 fF (1064 vesicles) and 237.0 fF (2963 vesicles) for endbulb and calyx terminals, respectively. The total number of readily releasable vesicles was thus ∼2.8 times larger for calyx terminals, which is consistent with their ∼4 times larger surface area (see above). This analysis neglects vesicle pool replenishment and may therefore overestimate the readily releasable pool (RRP) because of the contribution of newly recruited vesicles to ΔC_m. However, simple simulations using published replenishment rates suggest that this error is negligible (see the accompanying online Supplemental Material).

To estimate the fraction of vesicles released during single APs we 'back-calculated' the predicted ΔC_m in response to the simulated Ca^{2+} charge influx elicited by presynaptic APs (see Fig. 6*G*, Table 1). Such estimates indicated 20 fF (calyx) and 3.1 fF (endbulb) corresponding to 250 and 40 synaptic vesicles. Thus, the Ca^{2+} current charge entering the terminal during single APs triggers the release of <10% of the total RRP in both terminals.

Discussion

A large glutamatergic mammalian presynaptic terminal – the endbulb of Held – was characterized in depth in this study. Beyond demonstrating the feasibility of direct recordings from this presynaptic ending in acute brain slices, our study revealed several fundamental parameters including passive membrane properties and the kinetics of presynaptic APs. We studied gating characteristics of VGCCs and estimated their unitary current amplitudes to approximate the number of VGCCs per terminal. We used a combination of electrophysiological recordings together with modelling to study AP-evoked Ca^{2+} influx at the endbulb synapse. Finally, we used capacitance measurements to estimate the number of readily releasable vesicles.

Although all endbulbs are large axosomatic endings, they can vary considerably in shape (Ryugo & Fekete,

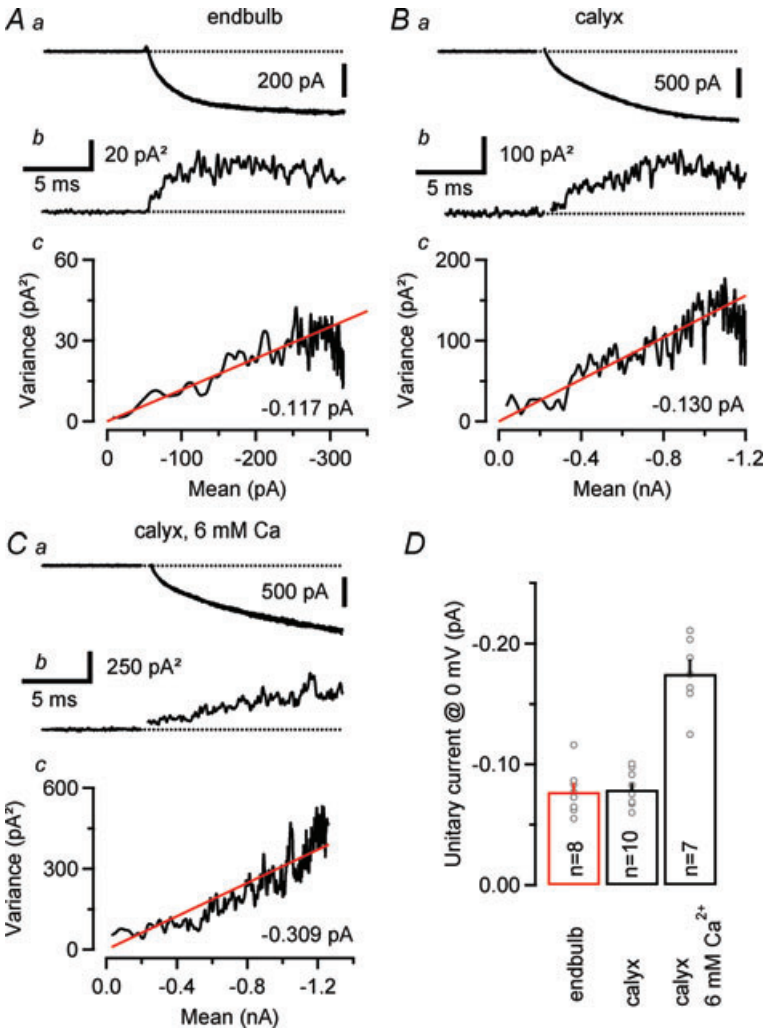

Figure 7. Single channel current of VGCCs expressed in endbulb and calyx terminals
Ensemble variance–mean analysis of $I_{Ca(V)}$ recorded at relatively low V_m in an endbulb (*A*, $V_m = -13$ mV, 74 repetitions) and two calyx synapses at 2 mM (*B*, $V_m = -15$ mV, 65 repetitions) and 6 mM (*C*, $V_m = -10$ mV, 65 repetitions) external Ca^{2+}. Seven consecutive sweeps are shown superimposed in the top row (*Aa*, *Ba* and *Ca*). The corresponding variance traces are shown below (*Ab*, *Bb* and *Cb*). Variance was estimated from difference traces (eqn (10)) to optimally eliminate trends and drifts, and background variance was subtracted. *Ac*, *Bc* and *Cc*, variance–mean plots for the same terminals. Red lines represent linear fits to the initial slop after the variance was corrected for the contribution from the background. The estimated unitary currents *i* were –0.117 pA, –0.130 pA and –0.308 pA for the endbulb and the two calyx terminals, respectively. *D*, summary data obtained from 8 endbulbs and 10 calyces. The expected unitary current amplitudes at $V_m = 0$ mV (*i*(0)) were calculated according to eqn (12). For comparison, the estimated *i*(0) at elevated external Ca^{2+} (6 mM) is shown.

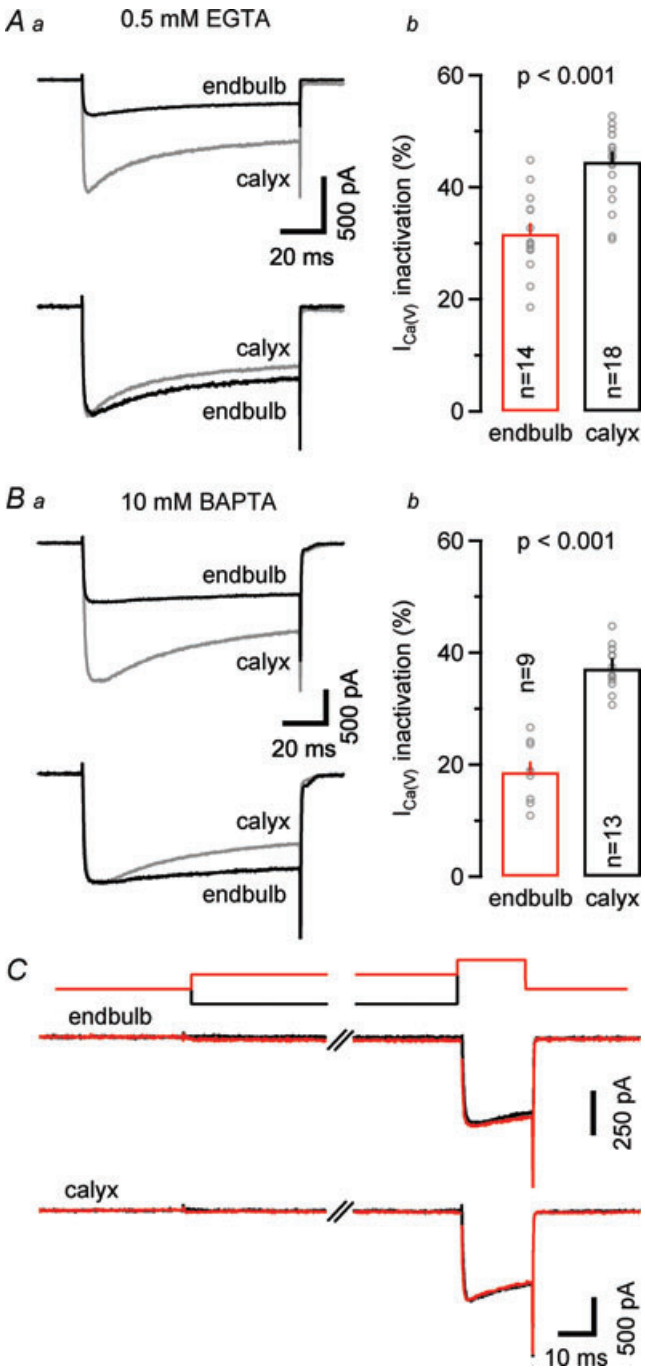

Figure 8. Inactivation of presynaptic $I_{Ca(V)}$ during sustained depolarizations is significantly less at endbulb *versus* calyx terminals
Aa, representative recordings of $I_{Ca(V)}$ (100 ms depolarization to 0 mV) from an endbulb (black) and a calyx (grey) terminal (top panel) recorded with a pipette solution containing 0.5 mM EGTA. Both currents were normalized with respect to their peak amplitudes for comparison (bottom panel). *Ab*, comparison of fractional inactivation ($(I_{peak} - I_{100ms})/I_{peak}$) × 100%) in endbulb and calyx terminals. On average, $I_{Ca(V)}$ showed less inactivation in endbulb terminals *versus* calyx terminals. *Ba*, similar recordings as illustrated in *Aa*, but with 10 mM BAPTA in the internal recording solution. *Bb*, under these recording conditions, the amount of $I_{Ca(V)}$ inactivation was only slightly attenuated in calyx terminals but profoundly reduced in endbulbs. *C*, steady-state inactivation of $I_{Ca(V)}$ was nearly negligible in endbulb (middle traces) and calyx (bottom traces) terminals. $I_{Ca(V)}$ was elicited by a 20 ms pulse to 0 mV after conditioning depolarization (500 ms duration) to –120 mV (black) or –40 mV (top traces).

1982). We cannot exclude that different morphological categories of endbulb terminals also differ in their functional properties. Endbulbs arising from auditory fibres having low spontaneous discharge rates have been reported to have a more complex shape than those of high discharge rates (Ryugo & Sento, 1991). In addition, at the age P9–11, mouse endbulb terminals have not yet acquired their mature morphology (Neises *et al.* 1982; Limb & Ryugo, 2000) and further developmental changes in their functional properties are likely to occur. At the rat endbulb→bushy cell synapse, the average number of quanta released by a single AP increases considerably from ∼40 to ∼70 during the first three postnatal weeks (Bellingham *et al.* 1998), which is in line with the developmental increase in RRP size reported for mouse endbulb terminals (McKay & Oleskevich, 2007).

Unequivocal identification of endbulb terminals

We recorded from relatively young endbulb terminals which have a cup-shaped morphology and only a few filopodia arising from their main swelling (Limb & Ryugo, 2000). This compact morphology facilitates identification of the presynaptic terminals in acute slices and may be advantageous during voltage-clamp experiments. In some experiments we used fluorescent dyes to verify pre- or post-synaptic recording sites. However, because of their distinct passive membrane properties, recordings from endbulbs and bushy cells can be easily distinguished without the use of fluorescent dyes. During most experiments, we took advantage of the capacitance jump observed in response to membrane depolarization as an additional criterion to identify presynaptic terminals.

Heterogeneous size of endbulb terminals

We determined the membrane capacitance of endbulbs in comparison to calyces from the fast components of charging transients recorded under voltage-clamp. Assuming a specific membrane capacitance of 10 fF μm^{-2}, we estimate an average surface area of ∼430 μm^2 *vs.* 1720 μm^2 for endbulb and calyx terminals, respectively. The area values are probably upper estimates because the charging of proximal parts of the axon may contribute to the fast capacitive current transients.

Our estimate for the total surface area of endbulb terminals is 2–4 times larger than those for hippocampal (40–110 μm^2, Rollenhagen *et al.* 2007) and

cerebellar mossy terminals (69–200 μm^2, Xu-Friedman & Regehr, 2003) based on serial electron microscopy, but considerably smaller than those for calyces of Held from mice (this study) or rats (~2400 μm^2, Borst & Sakmann, 1998*a*; ~2500 μm^2, Sätzler *et al.* 2002). Assuming a disc-like geometry for the two types of terminals and a height of ~1 μm (Ryugo & Fekete, 1982; Nicol & Walmsley, 2002; Taschenberger *et al.* 2002; Ryugo *et al.* 2006), our surface area estimates correspond to disc diameters of ~16 μm *versus* ~32 μm, thus representing ~20% *versus* ~41% of the total circumference of a contacted soma having a diameter of ~25 μm. The surface of such disc-like structures would represent ~22% *vs.* ~88% of the surface of the contacted neurons for endbulbs and calyces, respectively. These estimates seem reasonable because SBCs of the AVCN accommodate one to four presynaptic contacts (Ryugo & Sento, 1991; Nicol & Walmsley, 2002) whereas principal cells of the MNTB generally receive only a single calyceal input. Interestingly, the area covered by endbulb silhouettes in Golgi impregnations or horseradish peroxidase (HRP)-labelled terminals of the cat AVCN typically range from ~200 to ~400 μm^2 (Brawer & Morest, 1975; Ryugo & Sento, 1991), which comes close to the expected ~50% of the total surface area of endbulb terminals estimated in this study.

Fast presynaptic APs in endbulb terminals

A characteristic feature of auditory synapses is their ability to transmit reliably at high rates of stimulation. Brief presynaptic APs may help to generate fast release transients and rapid EPSCs, which are advantageous to accomplish this task. Indeed, calyceal APs acquire very rapid kinetics during postnatal development (Taschenberger & von Gersdorff, 2000; Erazo-Fischer *et al.* 2007). We found that endbulb APs have similar rapid kinetics. In fact, the average half-width of the endbulb APs was significantly shorter when compared to calyx APs recorded at the same age (see Fig. 6). The time course of endbulb APs is likely to further accelerate significantly at physiological temperature because the average AP half-with of the calyx of Held was reported to decrease by ~50% at physiological compared to room temperature (Borst & Sakmann, 1998*a*).

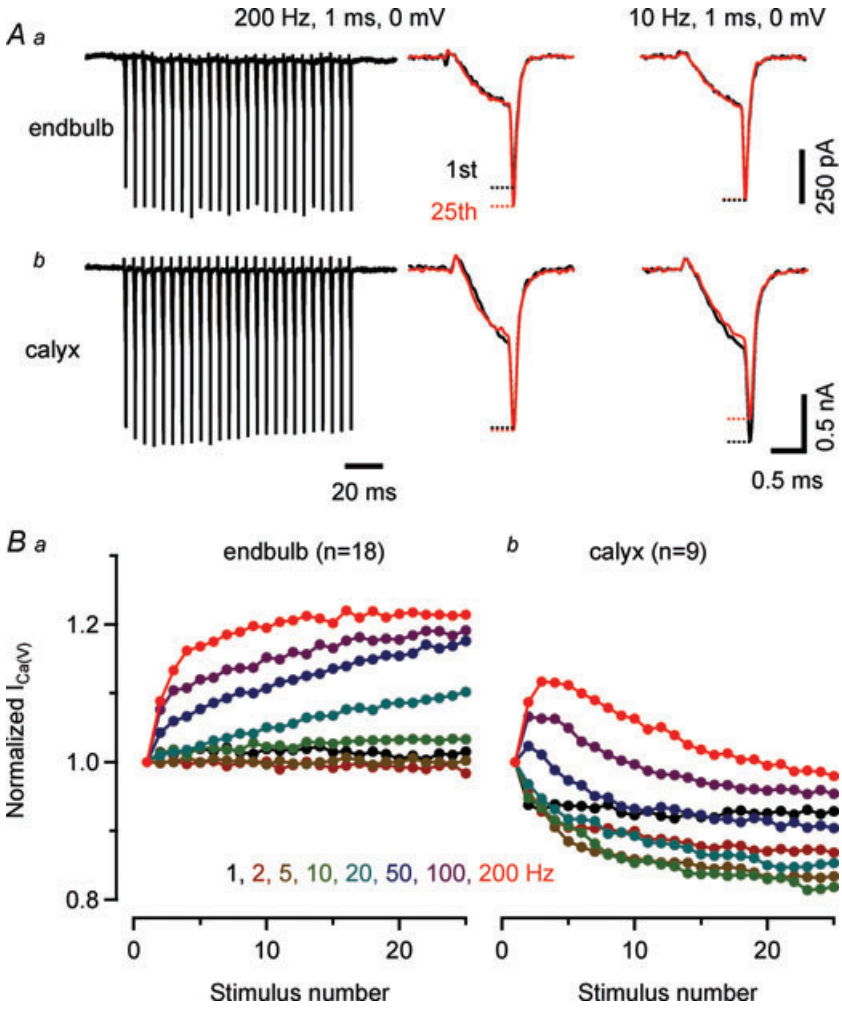

Figure 9. Presynaptic $I_{Ca(V)}$ at endbulb terminals facilitates and does not inactivate during trains of AP-like depolarizations
A, representative 200 Hz trains of $I_{Ca(V)}$ elicited by brief depolarizations (1 ms, 0 mV) recorded with a pipette solution containing 0.5 mM EGTA from an endbulb (*Aa*) and a calyx (*Ab*) terminal (left panel). Initial and final $I_{Ca(V)}$ are shown superimposed for comparison (middle panel). Facilitation of $I_{Ca(V)}$ was observed during train stimulation of endbulb terminal. In calyx terminals, $I_{Ca(V)}$ inactivated after initial facilitation. Low frequency stimulation (10 Hz) induced inactivation of $I_{Ca(V)}$ in calyx but not in endbulb terminals (right panel). *B*, facilitation and inactivation of presynaptic $I_{Ca(V)}$ during train stimulation at frequencies ranging from 1 to 200 Hz. Summary results from 18 endbulb (*Ba*) and 9 calyx terminals (*Bb*).

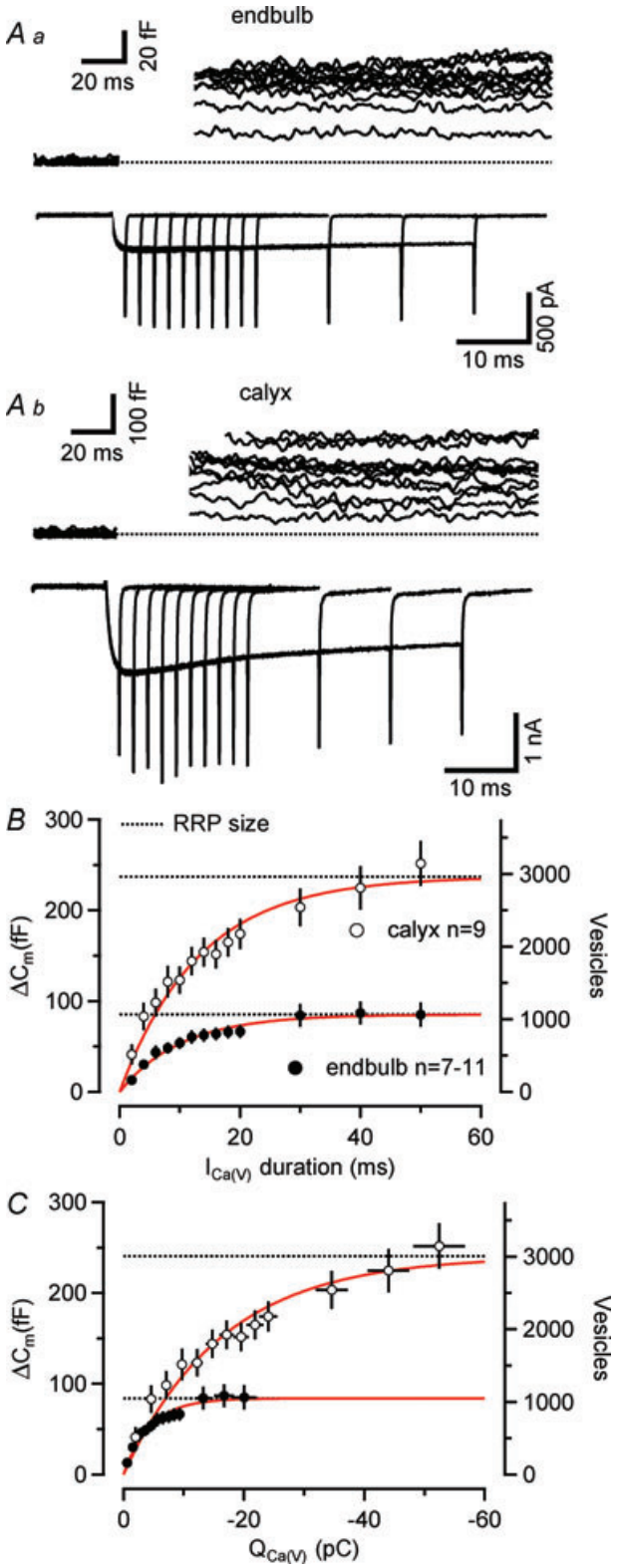

Figure 10. Readily releasable pool size is significantly smaller at endbulb compared with calyx terminals
A, series of depolarizing voltage steps (0 mV, duration from 2 to 50 ms) were applied to an endbulb (*Aa*) and a calyx (*Ab*) terminal. Top panels illustrate ΔC_m. Baseline levels of C_m, R_m and R_s were 3.81 pF, 1.24 GΩ and 16.7 MΩ and 22.2 pF, 6.09 GΩ and 11.5 MΩ for the endbulb and calyx recording, respectively. Corresponding $I_{Ca(V)}$ are shown in the bottom panels. *B* and *C*, changes in C_m plotted as a function of pulse duration (*B*) and presynaptic Ca^{2+} charge (*C*). The corresponding vesicle number (assuming 80 aF as the single vesicle capacitance, see results) are shown on the right axis. ΔC_m saturated for depolarizing voltage steps ≥40 ms. Smooth red lines represent single exponential fits. Estimates for the total number of readily releasable vesicles (dotted lines) were derived from the amplitudes of the exponentials.

It should be noted that presynaptic APs evoked by afferent fibre stimulation had slightly faster kinetics than those evoked by current injection. A similar tendency towards shorter half-width for fibre stimulation-evoked APs was also observed for mossy fibre boutons (Bischofberger *et al.* 2002). Interestingly, during prolonged depolarizations by current injection, endbulb terminals generally generated only single APs, which is reminiscent of the behaviour of more mature calyx terminals (Nakamura & Takahashi, 2007). These findings may indicate that endbulb terminals are slightly advanced in their functional maturation with respect to calyx of Held terminals at the same age. This would not be surprising because initial contact between endbulb terminals and SBCs is established before birth (Neises *et al.* 1982) but only at ∼P2 for the calyx of Held terminal and principal MNTB neuron (Hoffpauir *et al.* 2006; Rodriguez-Contreras *et al.* 2008).

Rapidly gating Ca^{2+} channels in endbulb terminals

Amplitudes of $I_{Ca(V)}$ were on average 3 times smaller in endbulb compared to calyx terminals which is consistent with the much smaller size of endbulb terminals (see Fig. 4). In contrast, Ca^{2+} current densities were relatively similar for the two types of terminals studied here and also in comparison to hippocampal mossy fibre boutons (Bischofberger *et al.* 2002) suggesting that this parameter may be relatively uniform among mammalian central synapses.

$I_{Ca(V)}$ at endbulb terminals activated at slightly more negative V_m when compared to that of calyx terminals. This could be related to the finding that the endbulb $I_{Ca(V)}$ was dominated by P/Q-type channels which seem to have a steady-state activation curve with a slightly more negative midpoint potential when compared to N-type VGCCs (Ishikawa *et al.* 2005; Li *et al.* 2007). Calyx terminals of the same age may express a higher fraction of N-type VGCCs (Wu *et al.* 1999). At P10, ∼75% of $I_{Ca(V)}$ was contributed by P/Q-type channels in calyces (Iwasaki *et al.* 2000) whereas the fraction of ω-AgaTX-sensitive VGCCs was ∼86% at endbulb terminals (Fig. 3*A*) (see also Oleskevich & Walmsley, 2002).

In order to approximate the total number of Ca^{2+} channels expressed at endbulb and calyx terminals, we

estimated the unitary conductance i of VGCCs by means of variance–mean analysis. Our estimates for i at $V_h = 0$ mV were similar for endbulb and calyx terminals but slightly smaller than those obtained at mossy fibre boutons (Li *et al.* 2007). We estimate an average number of 6400 and 20,400 VGCCs expressed at endbulb and calyx terminals, respectively. These numbers likely represent lower limits because we assumed an open probability of $\geq$0.8 at $V_m = 0$ mV. However, single channel recordings indicate that even at very high V_m, the open probability of VGCCs is probably substantially lower than 1 (Colecraft *et al.* 2001). Indeed, the variance–mean relationship for $I_{Ca(V)}$ measured at around −20 mV was well fitted by a linear regression (see Fig. 7), suggesting a relatively low open probability of VGCCs at this membrane potential.

The activation of endbulb VGCCs was very rapid with time constants <0.5 ms at positive membrane potentials and therefore allows the presynaptic AP to trigger brief and large calcium influx. To simulate AP-driven Ca^{2+} influx at endbulb terminals, we derived a HH-type m^2 model (Borst & Sakmann, 1998a). We estimate that ∼50% of all activatable channels are open at the peak of $I_{Ca(V)}$ during an AP. This number is considerably larger for mouse (∼90%, see Fig. 6) or rat (∼70%, Borst & Sakmann, 1998*a*) calyx terminals because of their wider presynaptic APs at this age. At physiological temperature, the AP half-width is much briefer compared to room temperature. This is, however, largely compensated by faster Ca^{2+} channel activation and deactivation kinetics (Nobile *et al.* 1990) such that the total calcium charge transfer decreases only slightly (Borst & Sakmann, 1998*a*). Because of the large number of expressed Ca^{2+} channels and their effective opening by presynaptic endbulb APs, it is likely that multiple VGCCs control the release of a single transmitter vesicle at the endbulb of Held synapse, similarly as has been suggested for calyx terminals (Borst & Sakmann, 1998a).

Absence of $I_{Ca(V)}$ inactivation during AP-like trains

During long-lasting tetanic stimulation of calyx synapses at high rates, $I_{Ca(V)}$ inactivates substantially (Forsythe *et al.* 1998) and this Ca^{2+}-dependent inactivation of VGCCs can contribute to synaptic depression (Xu & Wu, 2005). In endbulb terminals, $I_{Ca(V)}$ showed robust facilitation during trains of short AP-like depolarizations especially at stimulus frequencies $\geq$20 Hz (Borst & Sakmann, 1998*b*; Cuttle *et al.* 1998). No indication for $I_{Ca(V)}$ inactivation was observed. Thus, synaptic depression at endbulb terminals may be largely mediated by vesicle depletion and/or postsynaptic receptor desensitization (Yang & Xu-Friedman, 2008; Chanda & Xu-Friedman, 2010) rather than presynaptic Ca^{2+} channel inactivation as suggested recently by Wang *et al.* (2010). However, since the experiments illustrated in Fig. 9 were conducted at room temperature, we cannot exclude that more severe Ca^{2+} current inactivation may contribute to synaptic depression at physiological temperature.

A large pool of releasable vesicles in endbulb terminals

We compared vesicle exocytosis at endbulb and calyx terminals using capacitance measurements which have the advantage of being independent of postsynaptic receptors and thus avoid non-linearities due to receptor saturation and desensitization. Well resolved capacitance jumps were obtained for depolarizations $\geq$2 ms. We estimate that the pool of readily releasable vesicles in endbulb terminals consists of ∼1060 vesicles. Thus, the pool is substantially larger than previously estimated using cumulative evoked EPSCs (Oleskevich *et al.* 2004). When normalizing the RRP size by terminal surface area ($C_{terminal}$), we estimate averages of 250 vesicles pF^{-1} and 170 vesicles pF^{-1} for endbulbs and calyces, respectively. This is much less than the 970 vesicles pF^{-1} that can be calculated for mossy fibre boutons (1400 vesicles/1.44 pF) (Hallermann *et al.* 2003).

Our RRP estimate of 1064 vesicles compares favourably to available EM data. Nicol & Walmsley (2002) reconstructed four endbulb terminals of a P25 rat from EM serial sections and reported an average number of 155 synaptic specializations per endbulb. The mean number of docked vesicles per synaptic specialization varied from 2.1 to 14.8 (mean ∼6.5). Using these values, we arrive at a total number of ∼1005 docked vesicles per endbulb which is surprisingly close to our RRP estimate.

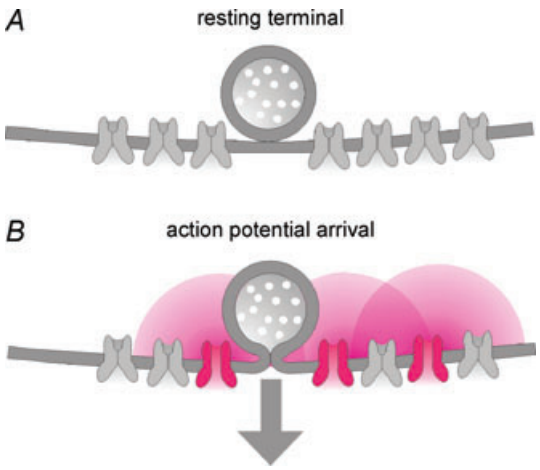

Figure 11. Putative arrangement of docked vesicles and VGCCs at endbulb active zones
A, based on our estimates for the number of docked vesicles as well as the number of VGCCs expressed in a single endbulb terminal, we propose that an average number of 7–8 VGCCs is associated with each docked vesicle at endbulb AZs. *B*, upon AP arrival, 3–4 VGCCs are opened at the peak of the AP-induced Ca^{2+} current.

Comparing our estimated number of readily releasable vesicles with the total number of VGCCs expressed in single terminals, we hypothesize that at least seven to eight (endbulb) and six to seven (calyx) VGCCs are associated with each docked vesicle (Table 1, Fig. 11). This ratio could be lower if a larger number of presynaptic VGCCs are located outside active zones (Wu *et al.* 1999). Upon arrival of a presynaptic AP, a maximum of three to four VGCCs will be opened at the peak of the AP-induced Ca^{2+} current. The average number of VGCCs controlling release of a single vesicle seems to decrease developmentally at the calyx of Held (Fedchyshyn & Wang, 2005; Wang *et al.* 2008). Interestingly, single hippocampal mossy fibre boutons are equipped with ∼1400 readily releasable vesicles (Hallermann *et al.* 2003) and express an average number of ∼2000 VGCCs (Li *et al.* 2007). Thus, only one to two VGCCs seem to co-localize with each docked vesicle in the mossy fibre bouton.

At the endbulb terminal, about half of the vesicles in the readily releasable pool (∼530 vesicles) could be released within the first ∼7 ms of a depolarization to 0 mV suggesting that multiple rounds of exocytosis occurred at individual active zones during this time. Since short, AP-like depolarizations triggered the release of <10% of the total RRP, release probability must be very low at the endbulb synapse. At the calyx of Held, a large fraction of docked vesicles seems to be located relatively distant from the sites of Ca^{2+} influx (Wadel *et al.* 2007) and vesicles of the RRP seem heterogeneous regarding their intrinsic properties (Wölfel *et al.* 2007). Thus, only part of the readily releasable vesicles contribute to the fast, synchronous release transients underlying AP-evoked EPSCs. It remains to be determined whether such heterogeneities exist in the endbulb of Held terminal, and how this shapes synaptic processing in the cochlear nucleus.

References

Augustine GJ (1990). Regulation of transmitter release at the squid giant synapse by presynaptic delayed rectifier potassium current. *J Physiol* **431**, 343–364.

Augustine GJ, Charlton MP & Smith SJ (1985). Calcium entry into voltage-clamped presynaptic terminals of squid. *J Physiol* **367**, 143–162.

Barnes-Davies M & Forsythe ID (1995). Pre- and postsynaptic glutamate receptors at a giant excitatory synapse in rat auditory brainstem slices. *J Physiol* **488**, 387–406.

Bellingham MC, Lim R & Walmsley B (1998). Developmental changes in EPSC quantal size and quantal content at a central glutamatergic synapse in rat. *J Physiol* **511**, 861–869.

Bischofberger J, Geiger JR & Jonas P (2002). Timing and efficacy of Ca^{2+} channel activation in hippocampal mossy fibre boutons. *J Neurosci* **22**, 10593–10602.

Borst JG, Helmchen F & Sakmann B (1995). Pre- and postsynaptic whole-cell recordings in the medial nucleus of the trapezoid body of the rat. *J Physiol* **489**, 825–840.

Borst JG & Sakmann B (1998*a*). Calcium current during a single action potential in a large presynaptic terminal of the rat brainstem. *J Physiol* **506**, 143–157.

Borst JG & Sakmann B (1998*b*). Facilitation of presynaptic calcium currents in the rat brainstem. *J Physiol* **513**, 149–155.

Borst JG & Sakmann B (1999). Effect of changes in action potential shape on calcium currents and transmitter release in a calyx-type synapse of the rat auditory brainstem. *Philos Trans R Soc Lond B Biol Sci* **354**, 347–355.

Brandt A, Khimich D & Moser T (2005). Few CaV1.3 channels regulate the exocytosis of a synaptic vesicle at the hair cell ribbon synapse. *J Neurosci* **25**, 11577–11585.

Brawer JR & Morest DK (1975). Relations between auditory nerve endings and cell types in the cat's anteroventral cochlear nucleus seen with the Golgi method and Nomarski optics. *J Comp Neurol* **160**, 491–506.

Brawer JR, Morest DK & Kane EC (1974). The neuronal architecture of the cochlear nucleus of the cat. *J Comp Neurol* **155**, 251–300.

Brown AM, Tsuda Y & Wilson DL (1983). A description of activation and conduction in calcium channels based on tail and turn-on current measurements in the snail. *J Physiol* **344**, 549–583.

Cant NB & Morest DK (1979). Organization of the neurons in the anterior division of the anteroventral cochlear nucleus of the cat. Light-microscopic observations. *Neuroscience* **4**, 1909–1923.

Chanda S & Xu-Friedman MA (2010). A low-affinity antagonist reveals saturation and desensitization in mature synapses in the auditory brain stem. *J Neurophysiol* **103**, 1915–1926.

Colecraft HM, Brody DL & Yue DT (2001). G-protein inhibition of N- and P/Q-type calcium channels: distinctive elementary mechanisms and their functional impact. *J Neurosci* **21**, 1137–1147.

Cuttle MF, Tsujimoto T, Forsythe ID & Takahashi T (1998). Facilitation of the presynaptic calcium current at an auditory synapse in rat brainstem. *J Physiol* **512**, 723–729.

Erazo-Fischer E, Striessnig J & Taschenberger H (2007). The role of physiological afferent nerve activity during in vivo maturation of the calyx of Held synapse. *J Neurosci* **27**, 1725–1737.

Fedchyshyn MJ & Wang LY (2005). Developmental transformation of the release modality at the calyx of held synapse. *J Neurosci* **25**, 4131–4140.

Forsythe ID, Tsujimoto T, Barnes-Davies M, Cuttle MF & Takahashi T (1998). Inactivation of presynaptic calcium current contributes to synaptic depression at a fast central synapse. *Neuron* **20**, 797–807.

Hagiwara S & Ohmori H (1982). Studies of calcium channels in rat clonal pituitary cells with patch electrode voltage clamp. *J Physiol* **331**, 231–252.

Hallermann S, Pawlu C, Jonas P & Heckmann M (2003). A large pool of releasable vesicles in a cortical glutamatergic synapse. *Proc Natl Acad Sci U S A* **100**, 8975–8980.

Heinemann SH & Conti F (1992). Nonstationary noise analysis and application to patch clamp recordings. *Methods Enzymol* **207**, 131–148.

Hessler NA, Shirke AM & Malinow R (1993). The probability of transmitter release at a mammalian central synapse. *Nature* **366**, 569–572.

Hodgkin AL & Huxley AF (1952). A quantitative description of membrane current and its application to conduction and excitation in nerve. *J Physiol* **117**, 500–544.

Hoffpauir BK, Grimes JL, Mathers PH & Spirou GA (2006). Synaptogenesis of the calyx of Held: rapid onset of function and one-to-one morphological innervation. *J Neurosci* **26**, 5511–5523.

Ishikawa T, Kaneko M, Shin HS & Takahashi T (2005). Presynaptic N-type and P/Q-type Ca^{2+} channels mediating synaptic transmission at the calyx of Held of mice. *J Physiol* **568**, 199–209.

Iwasaki S, Momiyama A, Uchitel OD & Takahashi T (2000). Developmental changes in calcium channel types mediating central synaptic transmission. *J Neurosci* **20**, 59–65.

Iwasaki S & Takahashi T (1998). Developmental changes in calcium channel types mediating synaptic transmission in rat auditory brainstem. *J Physiol* **509**, 419–423.

Joris PX, Carney LH, Smith PH & Yin TC (1994). Enhancement of neural synchronization in the anteroventral cochlear nucleus. I. Responses to tones at the characteristic frequency. *J Neurophysiol* **71**, 1022–1036.

Li L, Bischofberger J & Jonas P (2007). Differential gating and recruitment of P/Q-, N-, and R-type Ca^{2+} channels in hippocampal mossy fibre boutons. *J Neurosci* **27**, 13420–13429.

Limb CJ & Ryugo DK (2000). Development of primary axosomatic endings in the anteroventral cochlear nucleus of mice. *J Assoc Res Otolaryngol* **1**, 103–119.

Lin KH, Chen IW & Taschenberger H (2010). Functional properties of presynaptic voltage-gated Ca^{2+} channels expressed at the endbulb of Held synapse. *2010 Abstract Viewer/Itinerary Planner*, Programme No. 448.3. Society for Neuroscience, Washington, DC.

Lindau M & Neher E (1988). Patch-clamp techniques for time-resolved capacitance measurements in single cells. *Pflügers Arch* **411**, 137–146.

Llinas R, Sugimori M & Simon SM (1982). Transmission by presynaptic spike-like depolarization in the squid giant synapse. *Proc Natl Acad Sci U S A* **79**, 2415–2419.

Luebke JI, Dunlap K & Turner TJ (1993). Multiple calcium channel types control glutamatergic synaptic transmission in the hippocampus. *Neuron* **11**, 895–902.

McKay SM & Oleskevich S (2007). The role of spontaneous activity in development of the endbulb of Held synapse. *Hear Res* **230**, 53–63.

Murthy VN, Sejnowski TJ & Stevens CF (1997). Heterogeneous release properties of visualized individual hippocampal synapses. *Neuron* **18**, 599–612.

Nakamura T, Yamashita T, Saitoh N & Takahashi T (2008). Developmental changes in calcium/calmodulin-dependent inactivation of calcium currents at the rat calyx of Held. *J Physiol* **586**, 2253–2261.

Nakamura Y & Takahashi T (2007). Developmental changes in potassium currents at the rat calyx of Held presynaptic terminal. *J Physiol* **581**, 1101–1112.

Neher E (1998). Vesicle pools and Ca^{2+} microdomains: new tools for understanding their roles in neurotransmitter release. *Neuron* **20**, 389–399.

Neises GR, Mattox DE & Gulley RL (1982). The maturation of the end bulb of Held in the rat anteroventral cochlear nucleus. *Anat Rec* **204**, 271–279.

Nicol MJ & Walmsley B (2002). Ultrastructural basis of synaptic transmission between endbulbs of Held and bushy cells in the rat cochlear nucleus. *J Physiol* **539**, 713–723.

Nobile M, Carbone E, Lux HD & Zucker H (1990). Temperature sensitivity of Ca currents in chick sensory neurones. *Pflugers Arch* **415**, 658–663.

Oertel D (1999). The role of timing in the brain stem auditory nuclei of vertebrates. *Annu Rev Physiol* **61**, 497–519.

Oleskevich S & Walmsley B (2002). Synaptic transmission in the auditory brainstem of normal and congenitally deaf mice. *J Physiol* **540**, 447–455.

Oleskevich S, Youssoufian M & Walmsley B (2004). Presynaptic plasticity at two giant auditory synapses in normal and deaf mice. *J Physiol* **560**, 709–719.

Rhode WS & Greenberg S (1992). Physiology of the cochlear nuclei. In *The Mammalian Auditory Pathway: Neurophysiology*, ed. Popper AN & Fay RR, pp. 94–152. Springer, New York.

Roberts WM, Jacobs RA & Hudspeth AJ (1990). Colocalization of ion channels involved in frequency selectivity and synaptic transmission at presynaptic active zones of hair cells. *J Neurosci* **10**, 3664–3684.

Rodriguez-Contreras A, van Hoeve JS, Habets RL, Locher H & Borst JG (2008). Dynamic development of the calyx of Held synapse. *Proc Natl Acad Sci U S A* **105**, 5603–5608.

Rollenhagen A, Satzler K, Rodriguez EP, Jonas P, Frotscher M & Lubke JH (2007). Structural determinants of transmission at large hippocampal mossy fibre synapses. *J Neurosci* **27**, 10434–10444.

Rosenmund C, Clements JD & Westbrook GL (1993). Nonuniform probability of glutamate release at a hippocampal synapse. *Science* **262**, 754–757.

Ryugo DK & Fekete DM (1982). Morphology of primary axosomatic endings in the anteroventral cochlear nucleus of the cat: a study of the endbulbs of Held. *J Comp Neurol* **210**, 239–257.

Ryugo DK, Montey KL, Wright AL, Bennett ML & Pongstaporn T (2006). Postnatal development of a large auditory nerve terminal: the endbulb of Held in cats. *Hear Res* **216–217**, 100–115.

Ryugo DK, Pongstaporn T, Huchton DM & Niparko JK (1997). Ultrastructural analysis of primary endings in deaf white cats: morphologic alterations in endbulbs of Held. *J Comp Neurol* **385**, 230–244.

Ryugo DK & Sento S (1991). Synaptic connections of the auditory nerve in cats: relationship between endbulbs of held and spherical bushy cells. *J Comp Neurol* **305**, 35–48.

Ryugo DK, Wu MM & Pongstaporn T (1996). Activity-related features of synapse morphology: a study of endbulbs of held. *J Comp Neurol* **365**, 141–158.

Sabatini BL & Regehr WG (1997). Control of neurotransmitter release by presynaptic waveform at the granule cell to Purkinje cell synapse. *J Neurosci* **17**, 3425–3435.
Sakaba T & Neher E (2001). Quantitative relationship between transmitter release and calcium current at the calyx of Held synapse. *J Neurosci* **21**, 462–476.
Sala F (1991). Activation kinetics of calcium currents in bull-frog sympathetic neurones. *J Physiol* **437**, 221–238.
Sätzler K, Sohl LF, Bollmann JH, Borst JG, Frotscher M, Sakmann B & Lübke JH (2002). Three-dimensional reconstruction of a calyx of Held and its postsynaptic principal neuron in the medial nucleus of the trapezoid body. *J Neurosci* **22**, 10567–10579.
Sigworth FJ (1980). The variance of sodium current fluctuations at the node of Ranvier. *J Physiol* **307**, 97–129.
Sivaramakrishnan S & Laurent G (1995). Pharmacological characterization of presynaptic calcium currents underlying glutamatergic transmission in the avian auditory brainstem. *J Neurosci* **15**, 6576–6585.
Sun JY & Wu LG (2001). Fast kinetics of exocytosis revealed by simultaneous measurements of presynaptic capacitance and postsynaptic currents at a central synapse. *Neuron* **30**, 171–182.
Takahashi T & Momiyama A (1993). Different types of calcium channels mediate central synaptic transmission. *Nature* **366**, 156–158.
Taschenberger H, Leao RM, Rowland KC, Spirou GA & von Gersdorff H (2002). Optimizing synaptic architecture and efficiency for high-frequency transmission. *Neuron* **36**, 1127–1143.
Taschenberger H & von Gersdorff H (2000). Fine-tuning an auditory synapse for speed and fidelity: developmental changes in presynaptic waveform, EPSC kinetics, and synaptic plasticity. *J Neurosci* **20**, 9162–9173.
Wadel K, Neher E & Sakaba T (2007). The coupling between synaptic vesicles and Ca^{2+} channels determines fast neurotransmitter release. *Neuron* **53**, 563–575.
Walmsley B, Edwards FR & Tracey DJ (1988). Nonuniform release probabilities underlie quantal synaptic transmission at a mammalian excitatory central synapse. *J Neurophysiol* **60**, 889–908.
Wang LY, Neher E & Taschenberger H (2008). Synaptic vesicles in mature calyx of Held synapses sense higher nanodomain calcium concentrations during action potential-evoked glutamate release. *J Neurosci* **28**, 14450–14458.
Wang Y, Ren C & Manis PB (2010). Endbulb synaptic depression within the range of presynaptic spontaneous firing and its impact on the firing reliability of cochlear nucleus bushy neurons. *Hear Res* **270**, 101–109.
Wölfel M, Lou X & Schneggenburger R (2007). A mechanism intrinsic to the vesicle fusion machinery determines fast and slow transmitter release at a large CNS synapse. *J Neurosci* **27**, 3198–3210.
Wu LG, Westenbroek RE, Borst JG, Catterall WA & Sakmann B (1999). Calcium channel types with distinct presynaptic localization couple differentially to transmitter release in single calyx-type synapses. *J Neurosci* **19**, 726–736.
Wu SH & Oertel D (1984). Intracellular injection with horseradish peroxidase of physiologically characterized stellate and bushy cells in slices of mouse anteroventral cochlear nucleus. *J Neurosci* **4**, 1577–1588.
Xu-Friedman MA & Regehr WG (2003). Ultrastructural contributions to desensitization at cerebellar mossy fibre to granule cell synapses. *J Neurosci* **23**, 2182–2192.
Xu J & Wu LG (2005). The decrease in the presynaptic calcium current is a major cause of short-term depression at a calyx-type synapse. *Neuron* **46**, 633–645.
Yamashita T, Hige T & Takahashi T (2005). Vesicle endocytosis requires dynamin-dependent GTP hydrolysis at a fast CNS synapse. *Science* **307**, 124–127.
Yang H & Xu-Friedman MA (2008). Relative roles of different mechanisms of depression at the mouse endbulb of Held. *J Neurophysiol* **99**, 2510–2521.
Young ED & Oertel D (2004). The cochlear nucleus. In *The Synaptic Organization of the Brain*, 5 edn, ed. Shepherd GM. Oxford University Press, Oxford.

Author contributions

All experiments were performed at Max Planck Institute for Biophysical Chemistry. K.-H.L. and H.T. designed experiments. K.-H.L. collected, K.-H.L. and H.T. analysed and interpreted the data. All authors wrote the paper.

Acknowledgements

We are grateful to Erwin Neher for continuous support and critically reading an earlier version of this manuscript. We thank Dmitry Bibichkov, I-Wen Chen and Takeshi Sakaba for valuable discussions, F. Würriehausen for expert advice on programming, and S. Schmidt and I. Herfort for excellent technical assistance. S.O. is grateful for funding support from the Australian Deafness Research Foundation.